UCSF
UC San Francisco Electronic Theses and Dissertations

Title
Regulation of replicative immortality by GABPβ1L in TERT promoter mutant glioblastoma

Permalink
https://escholarship.org/uc/item/5xc6g6c6

Author
Mancini, Andrew Guy

Publication Date
2018

Peer reviewed|Thesis/dissertation

eScholarship.org Powered by the California Digital Library
University of California

Regulation of replicative immortality by GABPβ1L in *TERT* promoter mutant glioblastoma

by

Andrew Guy Mancini

DISSERTATION

Submitted in partial satisfaction of the requirements for the degree of

DOCTOR OF PHILOSOPHY

in

Biomedical Sciences

in the

GRADUATE DIVISION

of the

UNIVERSITY OF CALIFORNIA, SAN FRANCISCO

To my parents, Cindy and Sam

For encouraging me to always do my best and giving me the tools to succeed

ACKNOWLEDGEMENTS

UCSF has been a truly fantastic place to conduct my graduate studies. I was confident in my choice of graduate school from day one and have not regretted a single moment of choosing this institution to pursue my PhD. From the community to the research to the facilities, everything here has worked together to create the perfect environment to do high quality and impactful research.

First and foremost, I would like to thank my thesis advisor Joe Costello. Joe has been the ideal advisor in every way possible. He was always there to push me forward when things were going well and pick me back up when things were going poorly. He was able to let me have independence yet still be there as a mentor to ensure my development as a scientist in every facet of research. Furthermore, Joe has been the driving force behind making the lab being an enjoyable place to be by bringing in people who work well together and always stressing the importance of breaking up hard work with heavy relaxation. Thank you for everything Joe.

I would additionally like to thank my thesis committee members, Kyle Walsh and Bill Weiss. Both Kyle and Bill have been my resources behind the scenes for the past four years. They have been two people who I can bounce any idea off of, no matter how ridiculous it is, and still get valuable feedback and discussion. Their input and guidance has directly resulted in me conducting higher quality research than I would have without them. Additionally, their willingness to talk about important issues outside of research, such as career development, have made this entire PhD process much less frantic and more controlled than I ever could have expected.

I would also like to acknowledge those who have strongly influenced me to go into science, especially Michelle Whaley at the University of Notre Dame. Michelle was the first person to give me an opportunity to do research and push me to challenge myself every day by asking important scientific questions and setting goals for myself. She has been there to give me guidance from my first year at Notre Dame until this day and has molded me as a scientist in every way from how I write, to how I speak, to how I think. I do not know where I would be at this moment without Michelle, but I highly doubt I would have ever gone to graduate school without her influence.

I would like to thank the Biomedical Sciences Graduate program, especially Demian Sainz and Ned Molyneaux. The entire BMS staff, but in particular these two, have always been there since day one to ensure that I am meeting the requirements at every stage of progression throughout graduate school. They turned a potentially confusing process into something simple and streamlined and I thank them for that. Both Demian and Ned have also been outlets for me to talk to about both personal and professional matters throughout graduate school, acting as additional avenues for guidance and advice that have been integral to my success.

I am indebted to the original members of the Costello laboratory. In particular, thank you Lindsey Jones for encouraging me to rotate with Joe one hazy night at Yancy's Saloon and thank you Rob Bell - my mentor, friend, and scientific muse – for giving me the opportunity to succeed in the Costello lab. Every else - Tali Mazor, Brett Johnson, Alex Pankov, Emily Hamilton, Jeff Chang, Serah Choi, Josie Hayes, and Chibo Hong - thank you all for giving me a fantastic second home in the lab and helping me transition to graduate student life as a bright-eyed first year who did not know

anything at all. I would also like to thank the current members of the Costello laboratory: Drew McKinney, Alex Amen, Radhika Mathur, Giselle Lopez, Stephanie Hilz, Matt Grimmer, Nick Stevers, and KT Nguyen. All of you have been integral to my success scientifically and have provided a wonderful outlet for a bit of fun outside of science most Tuesdays and every other day. I would specifically like to thank Ana Xavier-Magalhaes, with whom all of this work was closely conducted with and who has put up with me since day one. We joined the Costello lab at the same time and have worked side-by-side these past four years through both success and failure. I could not have asked for a better partner throughout graduate school than you.

I would like to thank all of the friends I have made as part of the UCSF program. Special shout out to Roman Camarda and KT Nguyen for showing me a good time during recruitment and pressuring me to come to UCSF in the first place. People like Francesca Aloisio, Eric Wigton, John Gagnon, Ibs Ali, Buddy White, Sara Taylor, and Krystal Fontaine have always been there to made graduate school a bit more fun than I ever thought it could be. Also, I can't forget mriends outside of UCSF – John Stallings, Colleen McCartney, Rob Mustak, John Mundaden, Nick Macor, Clare Yarka – who have been there to support me for these past years even though we may not see each other quite as much as we would like. I would like to thank my best friend and girlfriend, Celine Mahieu, for always being there for me whether we were together in San Francisco or 5,500 miles apart in different parts of the world. You have provided me with some of the best times of my life and have been a constant source of strength and inspiration for me these past four years.

Finally, I would like to thank my family for their continuous support these past four years. To my brothers, Greg and Chris - although we are thousands of miles apart, thank you for always being available whenever I need it. To my parents, Sam and Cindy - thank you for giving me the opportunity to succeed from day one in this world. I could not have asked for better parents and cannot imagine what I would do without you two. Thank you constantly pushing me to be a better person and never giving up on me.

This work was done in collaboration with Ana Xavier-Magalhães and has been adapted and reprinted largely as it appears in:

Mancini A., Xavier-Magalhães A., Woods W.S., Nguyen K.-T., Amen A.M., Hayes J.L., Fellmann C., Gapinske M., McKinney A.M., Hong C., Jones L.E., Walsh K.M., Bell R.J.A., Doudna J.A., Costa B.M., Song J.S., Perez-Pinera P., Costello J.F. Disruption of the β1L isoform of GABP reverses glioblastoma replicative immortality in a *TERT* promoter mutation-dependent manner. *Cancer Cell.* 34(3):513-528.

Regulation of replicative immortality by GABPβ1L in *TERT* promoter mutant glioblastoma

Andrew G. Mancini

ABSTRACT

Telomeres are repetitive sequences of DNA that protect the ends of chromosomes and are gradually lost each cycle of cell division. In cells such as stem cells and germ cells, telomeres are indefinitely maintained through the use of the enzymatic complex telomerase. In order to achieve replicative immortality and form a tumor, cancer cells must find a way to replenish telomeres early on during tumorigenesis. The most common way that cancer cells enable immortality is by reactivating expression of the catalytic subunit, Telomerase Reverse Transcriptase (TERT), which is normally silenced in somatic cells. Activating mutations in the promoter region of *TERT* gene are the most common mechanism through which tumor cells reactivate telomerase, allowing for indefinite telomere maintenance and enabling cellular immortalization. These mutations specifically recruit the multimeric ETS factor GABP, which can form two functionally independent transcription factor species – a dimer or a tetramer.

We have identified GABPβ1L, the tetramer-forming isoform of GABP that is dispensable for normal development, as being specifically recruited to the mutant *TERT* promoter in glioblastoma cells. We show that genetic disruption of GABPβ1L results in *TERT* silencing in a *TERT* promoter mutation-dependent manner. Reducing *TERT* expression by disrupting GABPβ1L culminates in telomere loss and cell death through exclusively in *TERT* promoter mutant cells. Orthotopic xenografting of GABPβ1L-reduced, *TERT* promoter mutant glioblastoma cells rendered lower tumor burden and

longer overall survival in mice. These results highlight the critical role of GABPβ1L in enabling immortality in *TERT* promoter mutant glioblastoma.

TERT promoter mutations are the third most common mutation in human cancer, and the single most common mutation in glioblastoma. Understanding how the promoter mutation leads to tumor cell immortality could uncover potential targets to undermine immortality and reduce tumor growth. *TERT* promoter mutations selectively recruit the transcription factor GABP to activate *TERT* expression across multiple types of cancer. Our results suggest that the normally dispensable GABPβ1L isoform of GABP is a key to tumor cell immortality in *TERT* promoter mutant brain tumors. Therefore, inhibiting GABPβ1L may be an approach to reverse tumor cell immortality while sparing *TERT* promoter wild-type cells.

TABLE OF CONTENTS

LIST OF TABLES

CHAPTER 2: GABPβ1L REGULATES THE MUTANT *TERT* PROMOTER IN GLIOBLASTOMA

CHAPTER 3: DISRUPTION OF GABPβ1L FUNCTION IS SUFFICIENT TO REVERSE GLIOBLASTOMA REPLICATIVE IMMORTALITY IN A *TERT* PROMOTER MUTATION-DEPENDENT MANNER

LIST OF FIGURES

CHAPTER 2: GABPβ1L REGULATES THE MUTANT *TERT* PROMOTER IN GLIOBLASTOMA

CHAPTER 3: DISRUPTION OF GABPβ1L FUNCTION IS SUFFICIENT TO REVERSE GLIOBLASTOMA REPLICATIVE IMMORTALITY IN A *TERT* PROMOTER MUTATION-DEPENDENT MANNER

CHAPTER 1: INTRODUCTION

1.1 TELOMERES AND TELOMERASE

Telomeres are a highly regulated complex of tandem 'TTAGGG' repeats and their associated proteins at the ends of each chromosome (Blackburn et al., 2006; Counter et al., 1992). Telomeres maintain DNA integrity by protecting or "capping" the ends of chromosomes, but progressively shorten with each cell division due to lagging-strand synthesis (Chin et al., 1999; Fitzgerald et al.; 1999). Normal human cells have chromosomes with telomeres ranging from 3 kilobases to 10 kilobases in length, with significant heterogeneity in telomere length existing between individual cells and even individual chromosomes (Blackburn et al., 2006). In somatic cells that cannot replenish their telomeres, telomeres endow the cell with a finite lifespan that limits the amount of times the cell can divide (Kim et al., 1994; Shay and Wright, 2000). When a telomere reaches a critically short length, the protein components of the telomere can no longer stably bind to and protect the end of the chromosome (Capper et al., 2007; der-Sarkissian et al., 2004; Blackburn et al., 2006). The loss of the telomere protein cap allows the de-protected chromosome to be recognized by DNA damage repair machinery as a double stranded break, thus triggering TP53- and Rb-dependent cell cycle arrest and senescence (Saretzki et al., 1999; Whitaker et al., 1995).

However, certain cells such as stem cells and germ cells can maintain telomere length indefinitely by replenishing lost telomeric repeats using the telomerase enzymatic complex (Bryan and Cech, 1999; Counter et al., 1998). Telomerase is an RNA-dependent DNA polymerase that counteracts telomere attrition in stem cells and germ cells, thereby allowing these cells to achieve a state of "immortalization" and replicate indefinitely (Kim et al., 1994; Shay and Wright, 2000). The telomerase complex is

composed of the non-coding RNA template *TERC* and the catalytic subunit Telomerase Reverse Transcriptase (TERT) along with additional scaffolding and auxiliary proteins (Bryan and Cech, 1999; Counter et al., 1998). The transcriptional regulation of the telomerase reverse transcriptase (*TERT*) gene is a rate-limiting step in modulating telomerase activity in non-germ cells (Bryan and Cech, 1999; Counter et al., 1998). For example, in somatic cells *TERT* expression is silenced and therefore telomerase activity is absent. In contrast, the majority of stem cells exhibits robust expression of *TERT* and therefore possesses high levels of telomerase activity (Kim et al., 1994; Shay and Wright, 2000).

1.2 IMMORTALITY IN CANCER

Similar to stem cells and germ cells, tumor cells must too find a way to overcome telomere shortening in order to continue to proliferate and achieve immortality (Chin et al., 1999; Kim et al., 1994; Shay and Wright, 2000). The acquisition of replicative immortality during tumorigenesis can be found across all human tumors regardless of tissue of origin (Vinagre et al. 2013; Killela et al. 2013). The enabling of replicative immortality in cancer is typically an early event during tumor evolution, acting as a "gateway event" that can predispose tumor cells to further tumorigenic events, such as mutations in tumor suppressors or oncogenes (Chiba et al., 2017; Counter et al., 1992; Hackett et al., 2001). In the absence of TP53, terminal telomere shortening results in spontaneous telomere fusions, causing massive cell death (der-Sarkissian et al., 2004; Saretzki et al., 1999; Whitaker et al., 1995). Cells that emerge from this period of crisis

have acquired genomic instability and cellular immortalization, fundamental features of human tumors (Hackett et al., 2001).

Although normally silenced in somatic cells, *TERT* is aberrantly expressed in 90% of aggressive cancers, highlighting this as a hallmark of tumorigenesis (Chin et al., 1999; Kim et al., 1994; Saretzki et al., 1999; Shay and Wright, 2000). Reactivating telomerase enables cells with finite lifespan to achieve limitless proliferative potential and bypass cellular senescence induced by DNA replication-associated telomere shortening (Meyerson et al., 1997). Several mechanisms of *TERT* gene re-activation have been previously described across a breadth of cancer types. These mechanisms include activation via epigenetic mechanisms, activation via oncogenic signaling (e.g. MYC-mediated activation or WNT-mediated activation), *TERT* gene amplification, *TERT* structural variation, and *TERT* promoter mutation (Ohba et al., 2016; Horn et al., 2013; Huang et al., 2013; Ceccarelli et al., 2016). In order to re-activate telomerase and achieve immortality, a tumor cell typically uses only one of these mechanisms to re-express or amplify a single allele of the *TERT* gene.

Understanding mechanisms of aberrant *TERT* expression represents a crucial outstanding problem in cancer research. Reversal of immortalization is a largely unexplored but potentially valuable therapeutic approach to treating cancer. However, previous attempts to inhibit telomerase in human cancer have largely failed due to off-target toxicities associated with reversing immortality in non-tumor cells such as hematopoietic stem cells (Shay and Wright, 2006). Therefore, inhibition of telomerase through targeted disruption of one or more of these mechanisms of *TERT* re-expression may represent a promising avenue for tumor-specific inhibition of replicative immortality.

1.3 *TERT* PROMOTER MUTATIONS IN GLIOBLASTOMA

Non-coding mutations in the *TERT* promoter are the third most common somatic mutation in human cancer, revealing a potentially causal biological mechanism driving increased telomerase activity in tumors (Arita et al., 2013; Killela et al., 2013; Zehir et al., 2017). Initially discovered in cutaneous melanoma, *TERT* promoter mutations have since been identified in over fifty types of human cancers (Huang et al., 2013; Horn et al., 2013; Zehir et al., 2017). These mutations occur primarily in cancers hypothesized as arising from cell populations with low levels of self-renewal, such as hepatocytes or keratinocytes (Killela et al., 2013). Specifically, one of two positions in the *TERT* promoter, G228A or G250A, is mutated in many adult and pediatric CNS tumors, including 83% of primary *IDH* WT GBM and 80-97% of OD, making them the most recurrent single-nucleotide mutations observed in these cancer types (Vinagre et al., 2013; Arita et al., 2013; Killela et al., 2013; Zehir et al., 2017).

Both mutations are associated with increased *TERT* expression and telomerase activity, and have prognostic power in GBM (Spiegl-Kreinecker et al., 2015; Vinagre et al., 2013). These two *TERT* promoter mutations are nearly always mutually exclusive, heterozygous, and arise early on during tumorigenesis (Horn et al. 2013; Huang et al. 2013; Killela et al., 2013). Furthermore, in tumor cells bearing *TERT* promoter mutations, these mutations are necessary – albeit not sufficient – for achieving replicative immortality (Chiba et al., 2015; Chiba et al., 2017). Both G>A transitions generate an identical 11bp sequence that was hypothesized to generate a *de novo* binding site for an ETS transcription factor (Horn et al., 2013; Bell et al. 2015). Despite

these compelling findings and the importance of *TERT* in human cancer, the precise function of the mutations had remained elusive.

1.4 GABP-MEDIATED REGULATION OF THE MUTANT TERT PROMOTER

We identified the functional consequence of these mutations to be recruitment of the ETS family transcription factor GA-binding protein (GABP) specifically to the mutant promoter (Bell et al., 2015). The cancer-specific interaction of GABP with the *TERT* core promoter mutations highlights a common mechanism utilized by many cancers to overcome replicative senescence (Bell et al., 2015; Stern et al., 2015; Makowski et al.; 2016). Although many ETS transcription factors can bind similar DNA sequence motifs, GABP is unique among all ETS factors in that it is an obligate multimer consisting of the DNA-binding GABPα subunit and trans-activating GABPβ subunit (Rosmarin et al., 2004; Sawada et al., 1994). GABP can act as a heterodimer (GABPαβ) composed of one GABPα and one GABPβ subunit or a heterotetramer ($GABP\alpha_2\beta_2$) composed of two GABPα and two GABPβ subunits (de la Brousse et al., 1994; Rosmarin et al., 2004).

Two distinct genes encode the GABPβ subunit: the *GABPB1* gene encoding GABPβ1 and the *GABPB2* gene encoding GABPβ2. The GABPβ1 subunit has two distinct isoforms, a short GABPβ1S isoform and a longer GABPβ1L isoform, while the GABPβ2 subunit has a single isoform. Whereas the GABPβ1S isoform is only able to dimerize with GABPα, both GABPβ1L and GABPβ2 possess a C-terminal leucine-zipper domain (LZD) that mediates the tetramerization of two GABPαβ heterodimers (de la Brousse et al., 1994; Rosmarin et al., 2004). Although GABPβ1L or GABPβ2 can form the GABP tetramer, GABP tetramers containing only the GABPβ1L isoform are functionally distinct from GABPβ2-containing tetramers and may control separate

transcriptional programs (Jing et al., 2008; Yu et al., 2012). Furthermore, while abolishing full GABP function results in early embryonic lethality in mice (Yu et al., 2012), inhibition of the GABβ1L-only tetramer-specific transcriptional program has minimal phenotypic consequences in a murine system (Jing et al., 2008; Xue et al., 2008). Thus, if the GABP tetramer-forming isoforms are necessary to activate the mutant *TERT*p, targeting these isoforms may be a viable therapeutic approach to selectively inhibit *TERT* and reverse replicative immortality in *TERT*p mutant cancer.

However, it is currently unclear whether the GABP tetramer-forming isoforms are necessary to activate the mutant *TERT* promoter or whether the GABP dimer is sufficient. Two proximal GABPα binding sites are required to recruit a GABP$\alpha_2\beta_2$ tetramer, and, interestingly, the *TERT* promoter has native ETS binding sites upstream of the hotspot mutations that are required for robust activation of the mutant promoter (Bell et al., 2015). These native ETS binding sites are located approximately three and five helical turns of DNA away from the C228T and C250T mutation sites, respectively, which is consistent with the optimal spacing for the recruitment of the GABP tetramer (Bell et al., 2015; Chinenov et al., 2000; Yu et al., 1997). Here we tested the hypothesis that the C228T and C250T hotspot promoter mutations recruit the tetramer-specific GABP isoforms to the mutant *TERT* promoter to enable telomere maintenance and replicative immortality.

CHAPTER 2: GABPβ1L REGULATES THE MUTANT *TERT* PROMOTER IN GLIOBLASTOMA

2.1 ABSTRACT

Single point mutations in the promoter region of the *Telomerase Reverse Transcriptase* (*TERT*) gene reactivate *TERT* expression and telomerase activity in cancer cells that bear them. These mutations create a consensus binding site for the multimeric ETS transcription factor GABP, allowing GABP to specifically bind to and activate the mutant *TERT* promoter either as a dimer or as a tetramer. Here, we show that genetic disruption of GABPβ1L, a tetramer-forming isoform of GABP that is dispensable for normal development, results in *TERT* silencing in a *TERT* promoter mutation-dependent manner. RNAi-mediated and LNA-ASO-mediated transient knockdown of GABPβ1L ubiquitously reduced *TERT* expression across a panel of *TERT* promoter mutant glioma lines, but had no effect in *TERT* promoter wild-type lines. Furthermore, reduction of GABPβ1L tetramerization ability via CRISPR-Cas9-mediated disruption of *GABPB1L* was sufficient to reduce GABP occupancy at the mutant *TERT* promoter as well as *TERT* expression exclusively in *TERT* promoter mutant lines. These data support GABPβ1L as the GABP isoform responsible for activating the mutant *TERT* promoter in glioblastoma.

2.2 THE GABP TETRAMER-FORMING ISOFORM GABPβ1L POSITIVELY REGULATES *TERT* EXPRESSION SOLELY IN *TERT* PROMOTER MUTANT TUMOR CELLS

To determine if the GABP dimer-forming isoform (GABPβ1S) or the tetramer-forming isoforms (GABPβ1L and GABPβ2) regulate the mutant *TERT* promoter, we performed gene knockdown experiments *in vitro* and expression correlation analysis in primary tumors. We used siRNA-mediated knockdown of GABPβ1 - affecting GABPβ1S and GABPβ1L - and GABPβ2 in three *TERT* promoter mutant glioma cell lines, six early passage primary cultures and five *TERT* promoter wild-type and *TERT* expressing cell lines. Knockdown of GABPβ1 significantly reduced *TERT* expression in eight of nine *TERT* promoter mutant cell cultures, but had limited effect in the *TERT* promoter wild-type cultures (Figure 1A). In contrast, siRNA-mediated knockdown of GABPβ2 had a less robust and more variable effect on *TERT* expression in *TERT* promoter mutant cells (Figure S1A).

We also tested whether the expression of *TERT* correlates with expression of specific GABP isoforms in clinical samples, including *TERT* promoter mutant GBMs and oligodendrogliomas. This analysis revealed a significant positive monotonic association between *TERT* and *GABPB1L* mRNA in both cancer types (Figure 1B), but no significant correlation between *TERT* and *GABPB1S* (Figure 1B) or *GABPB2* (Figure S1B) mRNA levels. Analysis of GABP isoform and *TERT* expression data in the predominantly *TERT* promoter wild-type colorectal cancer revealed no positive correlation between *TERT* expression and *GABPB1L* or *GABPB2* expression, although a positive correlation between *TERT* expression and *GABPB1S* expression was found

(Figure S1C). Due to the significant positive correlation between *GABPB1L* expression and *TERT* expression in glioma, we specifically looked for depletion of the tetramer-forming *GABPB1L* isoform mRNA in our β1 knockdown study and confirmed that this isoform mRNA was significantly depleted after siRNA-mediated knockdown in 13 of 14 cell lines (Figure 1C).

We further explored this potential dependence on the GABPβ1L isoform for activation of the mutant *TERT* promoter by directly knocking down GABPβ1L with a degradation-inducing Locked Nucleic Acid Anti-Sense Oligonucleotide (LNA-ASO) targeted to the *GABPB1L*-exclusive 3' UTR of the *GABPB1* transcript. This LNA-ASO specifically depleted *GABPB1L* transcript levels with no reduction in *GABPB1S* transcript levels (Figure S1D). LNA-ASO-mediated knockdown of GABPβ1L reduced *TERT* expression across all *TERT* promoter mutant cultures and had no effect on *TERT* expression in all *TERT* promoter wild-type cultures (Figure 1D). Taken together, these data support that the GABP tetramer-forming isoform GABPβ1L positively regulates *TERT* expression in *TERT* promoter mutant glioma.

2.3 CRISPR-CAS9-MEDIATED DISRUPTION OF *GABPB1L* REDUCES GABP-MEDIATED ACTIVATION OF THE MUTANT *TERT* PROMOTER

We then directly tested the necessity of GABPβ1L for mutant *TERT* promoter activation by generating clones with reduced GABPβ1L function from three of the aforementioned *TERT* promoter mutant GBM cell lines (GBM1, T98G, and LN229) and three *TERT* promoter wild-type control cell lines (NHAPC5, HCT116 and HEK293T) using nuclease-assisted vector integration (NAVI) CRISPR-Cas9 editing (Brown et al.,

2016; Gapinske et al., 2018) (Figure 2A). We isolated two independent *GABPB1L*-edited clones (C1 and C2) and one isogenic CRISPR control clone (CTRL) for each parental line using one of two non-overlapping sgRNAs targeting *GABPB1* exon 9 or a sgRNA targeting an intergenic region of chromosome 5, respectively (Figure S2A and Table S1). *GABPB1* exon 9 contains the coding sequence for the LZD, and disruption of this exon is sufficient for ablation of the GABPβ1L-containing tetramer while leaving GABPβ1S intact (Chinenov et al., 2000; Sawada et al., 1994). Each *GABPB1L*-edited clone had the disruption of at least one allele via integration of a puromycin or hygromycin resistance cassette with most remaining *GABPB1L* alleles containing indels in the LZD (Figure S2B and Table S2). Analysis of cassette integration and locus integrity at predicted off-target cutting sites in coding regions (Hsu et al., 2013) via PCR and Surveyor assay, respectively, showed no aberrations outside the target regions (Figures S3A-F). *GABPB1L*-edited clones had reduced GABPβ1L protein levels with no measurable reduction in β1S levels, further confirming the specificity of our editing approach (Figure S3G).

We next examined whether the indels in the remaining *GABPB1L* alleles (Figure S2B) were sufficient to generate GABPβ1L protein with reduced tetramerization activity. Using PCR-mediated site-directed mutagenesis, we replicated three mutations (Table S3) in *GABPB1L* and assayed the ability of the mutant GABPβ1L to form the GABP tetramer (Figure 2B). DEL1 and DEL2 are in-frame deletions in the *GABPB1L* LZD-coding region and DEL3 is a putative loss-of-function frame-shift mutation in the same domain (Figure S2B). Each of the tested mutations reduced the ability of GABPβ1L to form the tetramer compared to the wild-type control, thereby indicating that the

CRISPR-Cas9-induced mutations in the *GABPB1L* LZD-coding region are sufficient to produce variants of the GABP tetramer-forming isoform GABPβ1L with reduced function. Thus, all *GABPB1L*-edited clones will be referred to as "GABPβ1L-reduced" to encompass reductions in both protein levels and protein function.

Chromatin immunoprecipitation of GABP followed by quantitative PCR (qPCR) at the mutant *TERT* promoter revealed the loss of GABP binding in the GABPβ1L-reduced *TERT* promoter mutant clones compared to the control lines (Figure 2C). Furthermore, analysis of *TERT* expression via RT-qPCR confirmed a significant reduction in - but not complete loss of - *TERT* mRNA across all *TERT* promoter mutant clones, whereas no decreases in expression were detected in clones from *TERT* promoter wild-type cells (Figure 2D). Additionally, overexpression of exogenous GABPβ1L in each GABPβ1L-reduced clone was sufficient to rescue both *TERT* expression (Figures 2E and S3H) and GABP binding at the mutant *TERT* promoter (Figure 2F). Taken together, these data confirm that the GABP tetramer-forming isoform GABPβ1L is necessary for the complete activation of the mutant *TERT* promoter.

2.4 GABPβ1L REGULATES A SUBSET OF GABP TRANSCRIPTION FACTOR TARGETS IN GBM CELLS

We next explored whether canonical GABP target genes are affected at the expression level after inhibition of GABPβ1L function. The four targets selected for preliminary expression analysis (*COXIV*, *EIF6*, *RPS16*, and *TFB1M*) are essential for cell growth and have been previously identified to recruit the GABPβ1L-containing GABP tetramer via two ETS binding sites in their promoter (Carter and Avadhani, 1994;

Donadini et al., 2006; Genuario and Perry, 1996; Yang et al., 2014). *SKP2* contains only one ETS binding site in its promoter and should be unaltered by changes in GABPβ1L (Yang et al., 2007). We identified minimal differences in the expression of each of the five targets between the CRISPR control and GABPβ1L-reduced clones (Figure 3A).

To further interrogate the effects of GABPβ1L reduction on global gene expression, we performed RNA sequencing (RNA-seq) for our *TERT* promoter mutant CRISPR control and GABPβ1L-reduced lines 45 days post-editing (Figure 3B and Table S4). We identified 161 transcripts, including *TERT*, differentially expressed (DE; FDR<0.05) after GABPβ1L reduction that were common to all three *TERT* promoter mutant lines. A majority of these DE transcripts (55%) were transcribed from genes with GABP-bound promoters, as determined from ENCODE ChIP-seq data from *TERT* promoter wild-type and mutant cancer cell lines (see STAR Methods). Interestingly, however, the vast majority (99%) of GABP-bound genes were not differentially expressed between the control and β1L-reduced lines. Gene ontology analysis of these DE transcripts identified enrichment in genes involved in development, cell-to-cell signaling, and proliferation (Figure 3C and Table S5). This global transcriptional analysis further validates that we have significantly inhibited the function of GABPβ1L in the GABPβ1L-reduced cell lines. These data, in combination with our qPCR analysis of canonical GABP tetramer targets, supports previous studies delineating specific transcriptional programs that different GABP species may control (Jing et al., 2008; Xue et al., 2008; Yu et al., 2012). The basis for the differential sensitivity between the effects of disrupting GABPβ1L function on the mutant *TERT* promoter and selected down-regulated GABP loci relative to other GABP targets is unknown, but may be due to

compensation by GABPβ1S, GABPβ2, or other ETS factors at certain GABP binding sites and not at other sites, or due to cell type specific differences in the GABP transcriptional program. These data suggest that the GABP binding site created by mutations in the *TERT* promoter and a subset of GABP binding sites are more sensitive to inhibition of the GABPβ1L-containing GABP tetramer, while other GABP-bound sites are less sensitive.

2.5 MAIN FIGURES

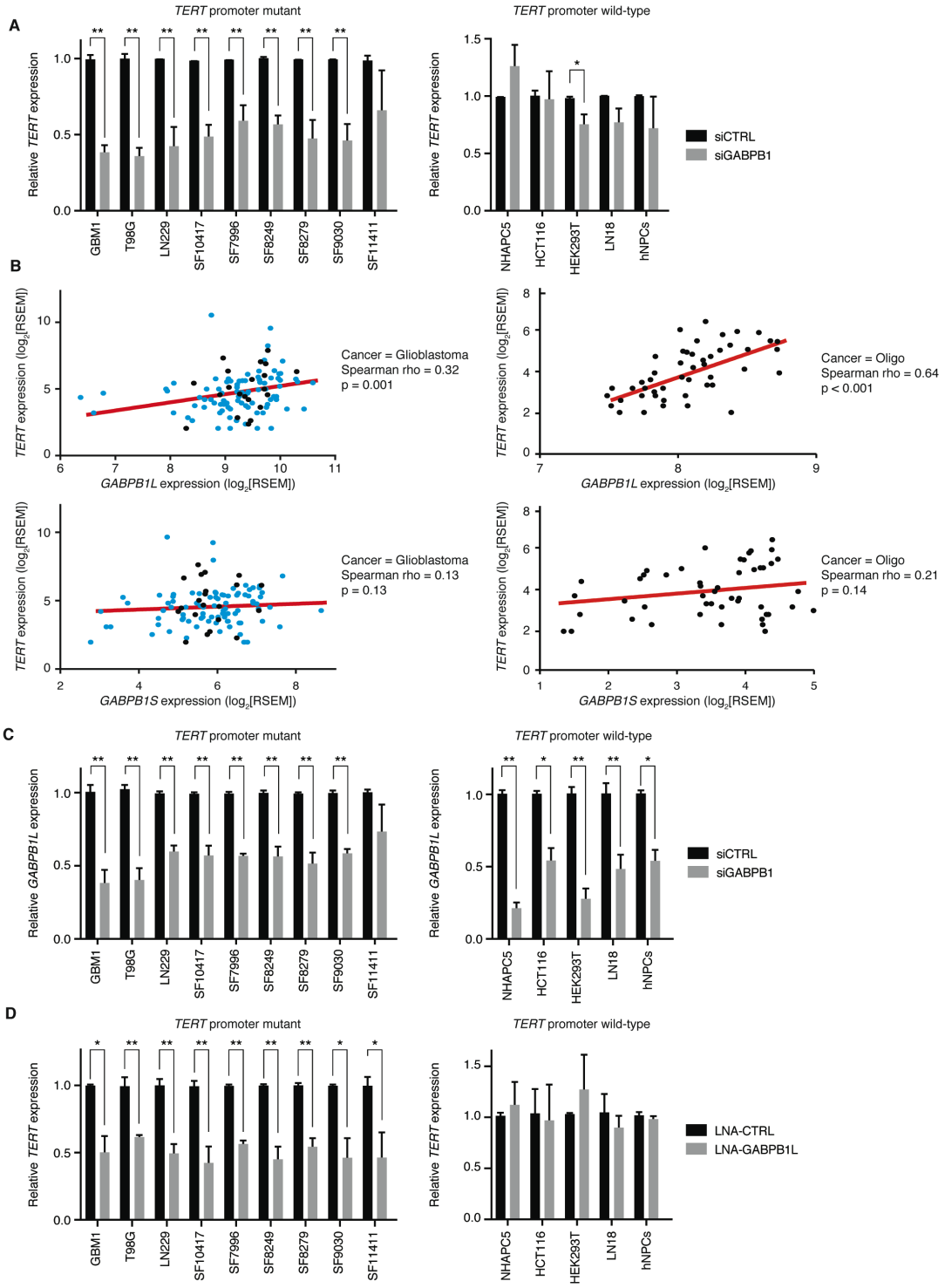

Figure 1. The GABP tetramer-forming isoform GABPβ1L positively regulates *TERT* expression solely in *TERT* promoter mutant tumor cells.

(A) *TERT* expression following siRNA-mediated knockdown of GABPβ1 (siGABPB1) in *TERT* promoter mutant (left) or *TERT* promoter-wild-type (right) cell lines and primary cultures. *p value<0.05, **p value<0.01, two-sided Student's t-test compared to a non-targeting siRNA control (siCTRL) in each respective line.
(B) Correlation of *GABPB1L* (top graphs) or *GABPB1S* (bottom graphs) expression (log_2[RSEM normalized counts]) versus *TERT* expression (log_2[RSEM normalized counts]) from 109 *TERT*-expressing GBMs (left graphs) or 49 *TERT* promoter-mutant oligodendrogliomas (right graphs). Red line indicates trend line. Black points indicate Sanger-validated *TERT* promoter mutant GBM and oligodendroglioma samples, teal points are GBM samples that were not tested for *TERT* promoter mutation status. Spearman's Rank-Order Correlation was used to generate Spearman rho and p values for each correlation.
(C) *GABPB1L* expression following siRNA-mediated knockdown of GABPβ1 (siGABPB1) in *TERT* promoter mutant (left) and wild-type (right) lines. *p value<0.05, **p value<0.01, two-sided Student's t-test compared to a non-targeting siRNA control (siCTRL) in each respective line.
(D) *TERT* expression following LNA-ASO knockdown of GABPβ1L (LNA-GABPB1L) in *TERT* promoter mutant (left) or wild-type (right) cell lines and primary cultures compared to a control LNA-ASO (LNA-CTRL). *p value<0.05, **p value<0.01, two-sided Student's t-test compared to LNA-CTRL in each respective line. Values are mean ± S.D. of at least three independent experiments (A, C, and D; two independent experiments for SF10417).
See also Figure S1.

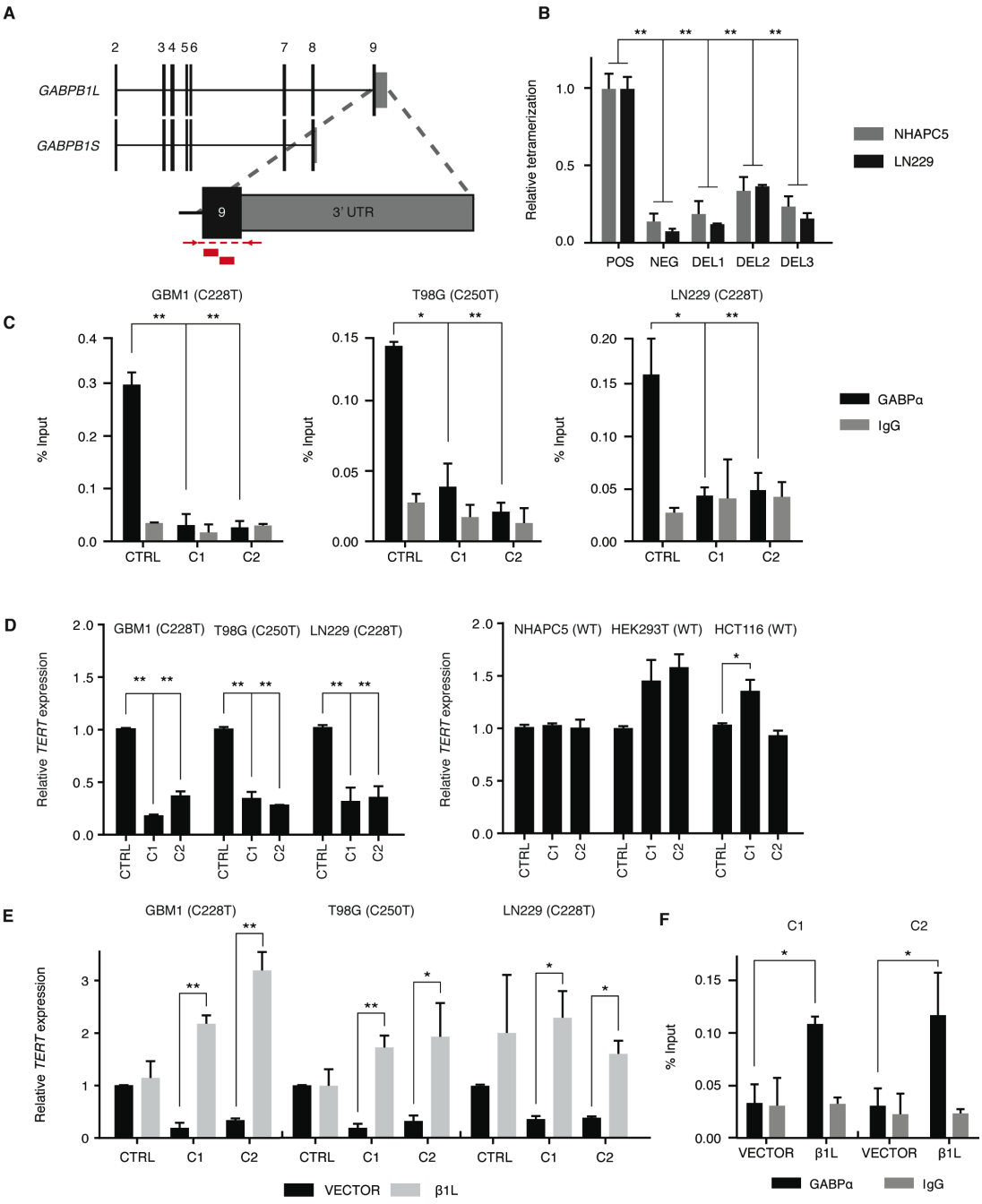

Figure 2. CRISPR-Cas9-mediated disruption of *GABPB1L* reduces GABP-mediated activation of the mutant *TERT* promoter.

(A) Exon structure for the *GABPB1* locus, depicting the *GABPB1S* and *GABPB1L* isoforms. Inset shows targeting strategy for CRISPR-Cas9 editing of *GABPB1L*. Red blocks indicate sgRNA target sites. Red arrows and dashed lines indicate primer locations and target amplicon for PCR validation of editing.

(B) Quantification of GABPβ1L tetramerization in the wild-type (POS) or mutated (DEL1-3) state. The negative (NEG) state consists of one GABPβ1L vector and one GABPβ1S vector, the products of which are unable to form a tetramer. *p value<0.05,

**p value<0.01, two-sided Student's t-test of DEL1-3 or NEG respective to the positive control (POS).
(C) GABPα or IgG control ChIP-qPCR for the *TERT* promoter in CRISPR control (CTRL) or β1L-reduced clones (C1 and C2). *p value<0.05, **p value<0.01, two-sided Student's t-test compared to respective CTRL.
(D) *TERT* expression relative to CTRL for GABPβ1L-reduced *TERT* promoter mutant (left) or wild-type (right) clones. *p value<0.05, **p value<0.01, two-sided Student's t-test compared to CTRL.
(E,F) *TERT* expression **(E)** or GABPα occupancy **(F)** in GABPβ1L-reduced clones relative to CTRL 48 hr following transfection with empty (VECTOR) or GABPβ1L expression vector. *p value<0.05, **p value<0.01, two-sided Student's t-test compared to respective VECTOR control.
Values are mean ± S.D. of at least two independent experiments (C and F) or three independent experiments (B, D, and E).
See also Figures S2-S3 and Tables S1-S3.

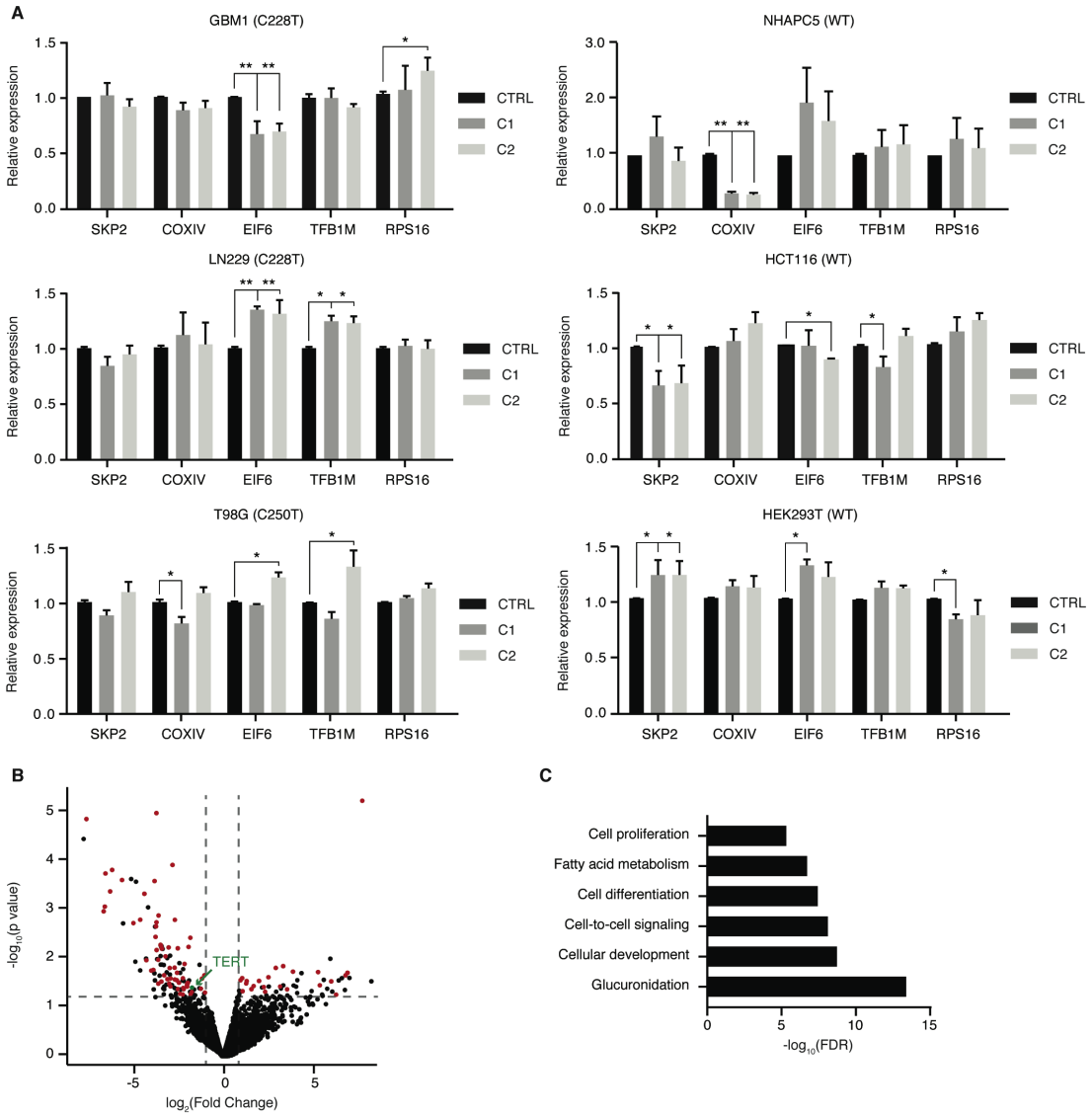

Figure 3. GABPβ1L regulates a subset of GABP transcription factor targets in GBM cells.

(A) Expression of one GABP dimer target and four GABP tetramer targets relative to CTRL for GABPβ1L-reduced clones derived from *TERT* promoter mutant and wild-type lines at day 45 post-editing. *p value<0.05, **p value<0.01, two-sided Student's t-test compared to CTRL. Values are mean ± S.D of at least three independent assays.

(B) Volcano plot of expression differences between CTRL and GABPβ1L-reduced *TERT* promoter mutant lines (GBM1, T98G, and LN229) as determined via RNA-seq at day 45 post-editing. Maroon-colored points represent putative GABP-regulated genes that are differentially expressed (log_2 Fold Change>1 & FDR<0.05).

(C) GO-terms analysis of 161 genes that are commonly differentially expressed genes between CTRL and multiple GABPβ1L-reduced *TERT* promoter mutant lines.

See also Tables S4 and S5.

2.6 SUPPLEMENTAL FIGURES

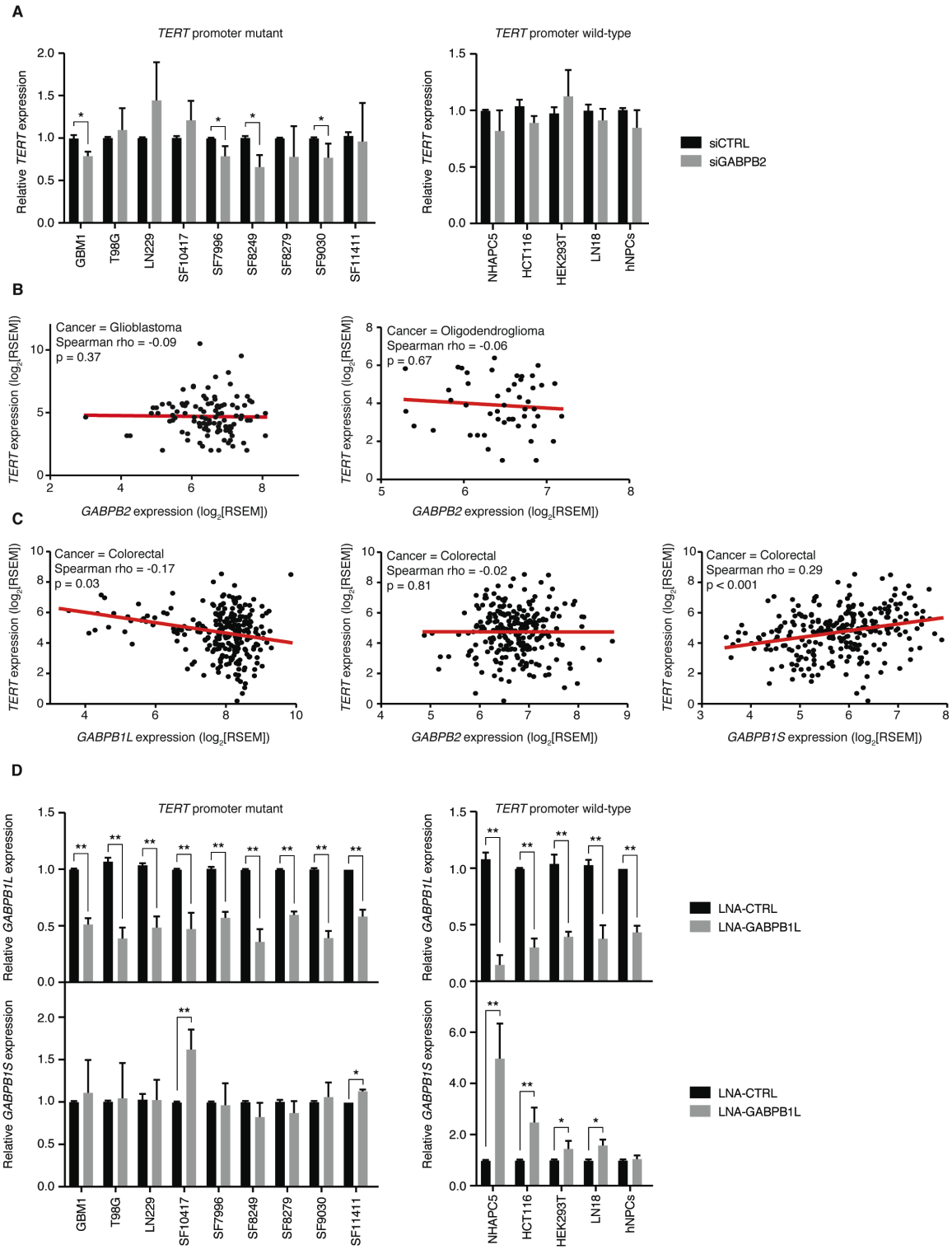

Figure S1, related to Figure 1. GABPβ1S and GABPβ2 do not robustly positively regulate *TERT* in *TERT* promoter mutant cancer with intact GABPβ1L.

(A) *TERT* expression following siRNA-mediated knockdown of GABPβ2 (siGABPB2) in *TERT* promoter mutant (left) or wild-type (right) cell lines and primary cultures. *p value<0.05, two-sided Student's t-test compared to a non-targeting siRNA (siCTRL) in each respective line.
(B,C) Correlation of *GABPB1L*, *GABPB1S*, or *GABPB2* mRNA expression (log_2[RSEM normalized counts]) versus *TERT* mRNA expression (log_2[RSEM normalized counts]) from 109 *TERT*-expressing GBMs and 49 *TERT* promoter-mutant oligodendrogliomas **(B)** and 262 *TERT*-expressing colorectal cancers **(C)**. Red line indicates trend line. Spearman's Rank-Order Correlation was used to generate Spearman's rho and p values for each monotonic correlation.
(D) *GABPB1L* and *GABPB1S* expression following LNA-ASO knockdown of β1L (LNA-GABPB1L) in *TERT* promoter mutant (left) or wild-type (right) cell lines and primary cultures compared to an LNA-ASO control (LNA-CTRL). *p value<0.05, **p value<0.01, two-sided Student's t-test compared to LNA-CTRL in each respective line.
All values are mean ± S.D. of at least three independent experiments (two independent experiments for SF10417 line).

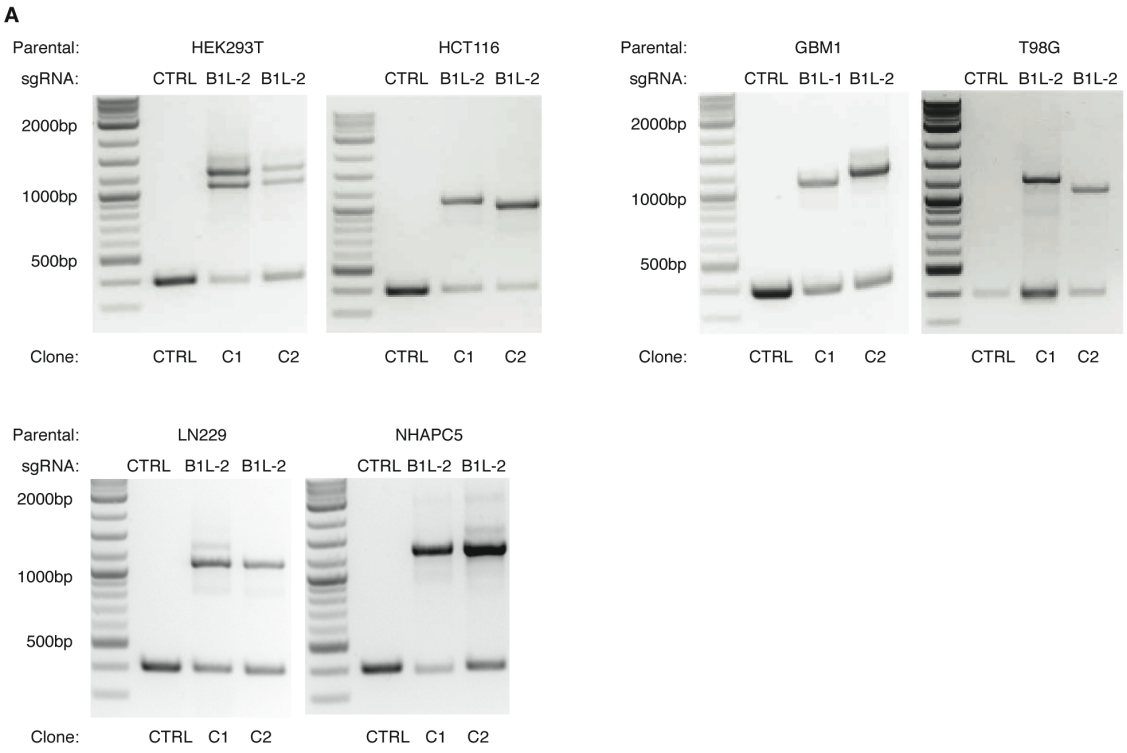

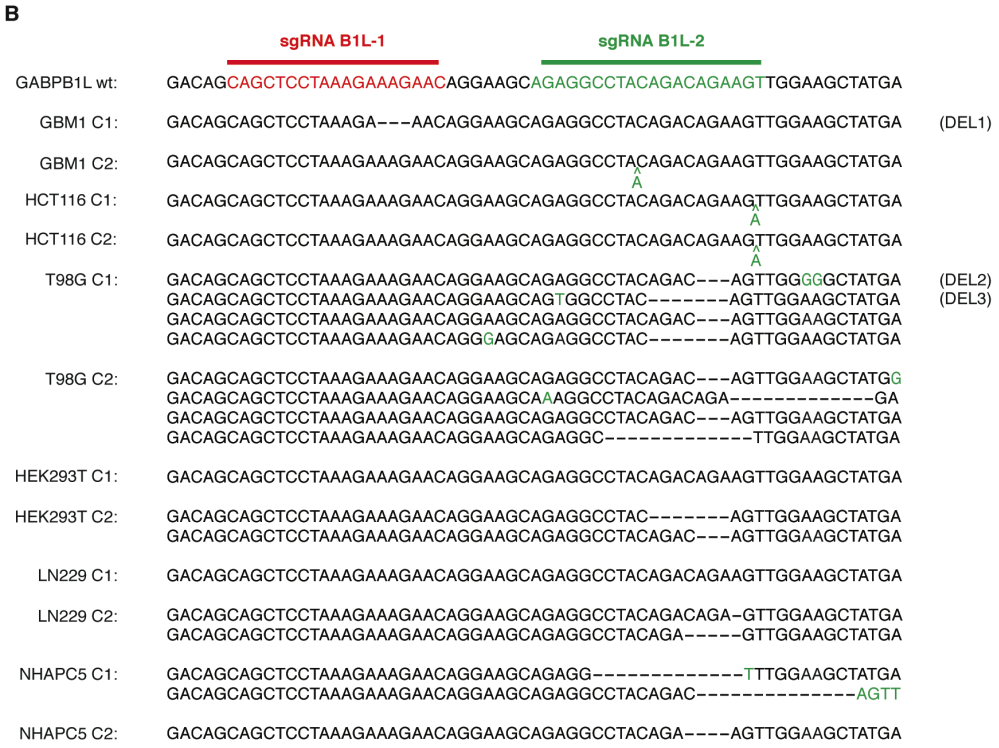

Figure S2, related to Figure 2. Validation of CRISPR-Cas9 editing.
(A) UV images of successful integration of the targeting vector (~1.1kb for forward integration, ~1.3kb for reverse integration) into exon 9 of *GABPB1* for the lines used in this study.

(B) Sanger sequencing of *GABPB1* exon 9 showing indels in alleles without targeting vector integration for each GABPβ1L-reduced clone. DEL1, DEL2, and DEL3 denote deletions induced in Figure 2B.

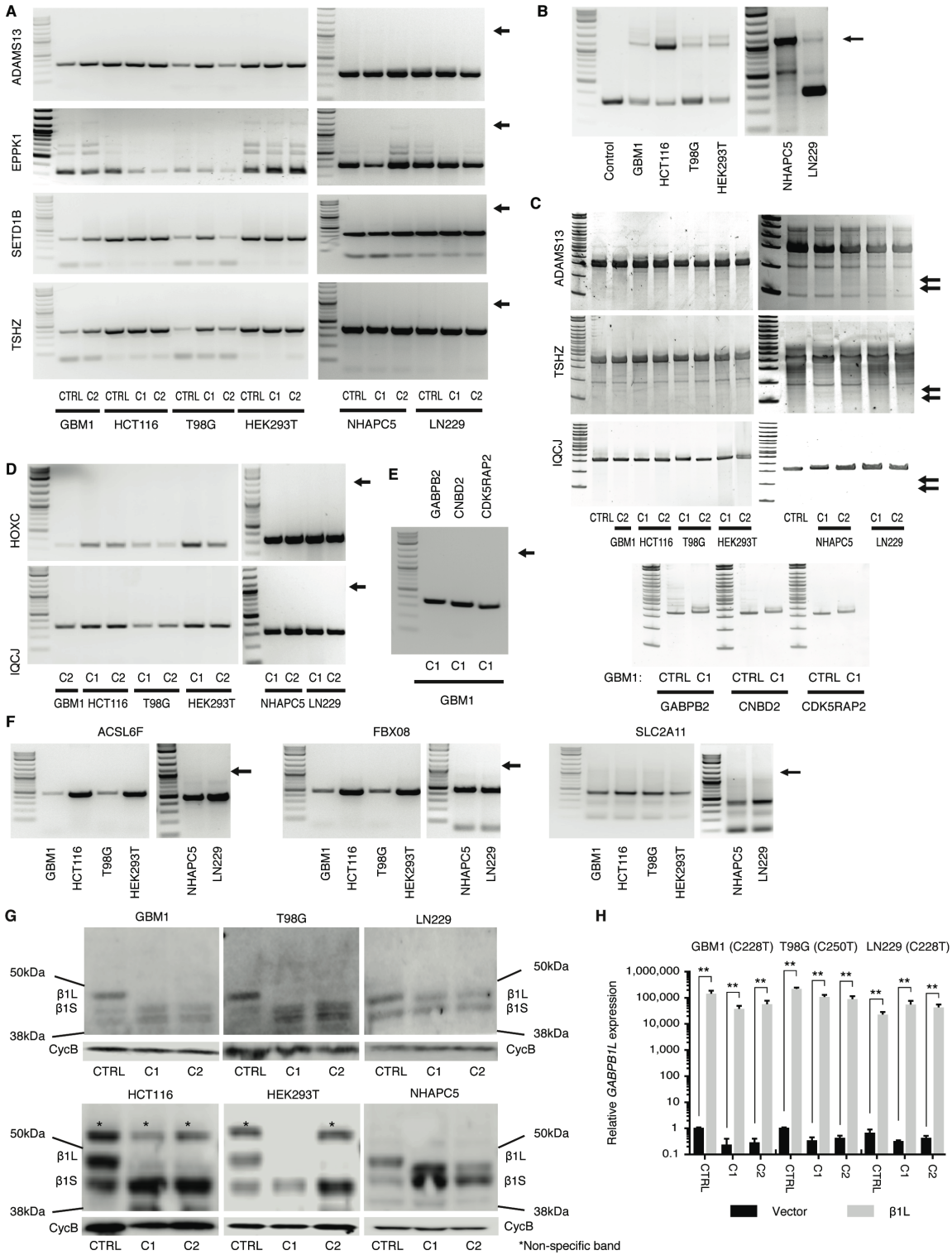

Figure S3, related to Figure 2. Validation of GABPβ1L protein reduction and analysis of potential off-target mutations introduced by CRISPR-Cas9 editing.

(A) PCR analysis for potential non-specific integration of the targeting vector at off-target coding regions for the universal sgRNA.
(B) On-target integration of the targeting vector at the negative control locus.
(C) Surveyor analysis to detect potential mutations introduced by CRISPR-Cas9 at coding sequences for all sgRNAs. Arrows indicate expected size of fragments from Surveyor assay if mutations are present.
(D-F) PCR analysis for potential non-specific integration of the targeting vector at off-target coding regions for *GABPB1L* sgRNA-2 **(D)**, *GABPB1L* sgRNA-1 **(E)** and control sgRNA **(F)**.
(G) Immunoblotting for GABPβ1 with GABPβ1L isoform (top, upper marked band) and GABPβ1S isoforms (top, lower marked bands) compared to a Cyclophilin B loading control (bottom) in all CRISPR-Cas9-edited cell lines. Asterisk (*) designates non-specific bands.
(H) *GABPB1L* expression in GABPβ1L-reduced clones relative to CTRL 48 hr following transfection with empty vector (VECTOR) or GABPβ1L expression vector. **p value<0.01, two-sided Student's t-test compared to respective VECTOR control.
Values are mean ± S.D. of three independent experiments.

2.7 SUPPLEMENTAL TABLES

Table S1, related to Figure 2. sgRNA sequences, targets, and PCR primers used for CRISPR-Cas9 editing.

Target	Location	Guide 1	Guide 2	PCR1-F	PCR1-R
GABPB1L	chr15:50,570,420-50,571,910	GCAGCTCCTAAAGAAAGAAC	AGAGGCCTACAGACAGAAGT	TGTGGAGCACAAAATTAGGG	CAAGATTGTATTCTTTCTTGACCAAA
CTRL	chr5:100,587,609-100,590,535	ATAATAATACGTACAGGCCC		GGTTCCTTCAGTACCCATGC	TCATACTTCCGGCTTTGGAG
Universal		ACCGGGTCTTCGAGAAGACC			TGCCCTTGTCTTGTAGTTTCC
Off-Target Locus					
GABPB2	chr1:151,070,578-151,125,542			CACCGCTCCTGGCCTGTCTTTT	GAGGCTCTGTGGTCCCTGCTGA
CNBD2	chr20:35,954,564-36,030,700			GGAGTGGAGTGGAGCTCTTGCC	GGGTCCCTCCTTTGTGCCATGC
CDK5RAP2	chr9:120,388,869-120,580,170			TCCTGAAGGTGGTGCTCTCT	TGTGTGTGTGTTCGCATTCA
HOXC	chr12:53,981,509-53,985,519			CCACAGTGGGGCTCAAGCTGTG	GCTTCTGGGGTGTGTTGAGGGC
IQCJ-SCHIP1	chr3:158,962,928-159,266,307			TCTTATGCCGCAGCCTATTT	AGTCAAGTGACAGAATCCACTGT
SETD1B	chr12:121,804,180-121,832,584			GGCACAGCGGCGAACTTCTCTT	TTGCAAACCACTCTGGGGCTGG
ADAMTS13	chr9:133,414,358-133,459,402			GGCAGGCACTTTTGTCACCCCA	CCCCACCTTGGCTGTGTGGTAC

Target	Location	Guide 1	Guide 2	PCR1-F	PCR1-R
TSHZ1	chr18:75,210,755-75,289,950			CGTGCAGCTCTACCGCCAGAAC	CCCGCTTTTTGGTGGAGGGGAC
EPPK1	chr8:143,857,324-143,878,464			CTGCGTGATGCCACCATGGAGG	TCCTGCAGCGTCTTAGTGCCCT
ACSL6	chr5:131,806,990-132,012,243			CCACACCCCAGGAGCAAAGATA	GCAGTCGCAGTATCCTCAGGAT
FBXO8	chr4:174,236,658-174,284,264			TTTTTCCCCACTCACTGGAGCA	GCCACCTGCCACAAAGTACAC
SLC2A11	chr22:23,856,703-23,886,309			GAGGCCAGAGTTTGAAACCAGC	CATGTACCACCACACCCAGCTA

Table S2, related to Figure 2. Summary of clones generated by CRISPR-Cas9 editing.

Parental	sgRNA	GABPB1L copy number	Clone #	GABPB1L allele 1	GABPB1L allele 2
GBM1	GABPB1L-1	2	1	Puro cassette insertion	3bp in-frame deletion
GBM1	GABPB1L-2	2	2	Puro cassette insertion	A frameshift insertion
T98G	GABPB1L-2	5	1	Puro cassette insertion	3bp in-frame deletion + AA>GG dinucleotide sub
T98G	GABPB1L-2	5	2	Puro cassette insertion	3bp in-frame deletion + A>G sub
LN229	GABPB1L-2	3	1	Puro cassette insertion	Puro cassette insertion
LN229	GABPB1L-2	3	2	Puro cassette insertion	1bp frameshift deletion
HCT116	GABPB1L-2	2	1	Puro cassette insertion	A frameshift insertion
HCT116	GABPB1L-2	2	2	Puro cassette insertion	A frameshift insertion
HEK293T	GABPB1L-2	3	1	Puro cassette insertion	Puro cassette insertion
HEK293T	GABPB1L-2	4	2	Puro cassette insertion	Puro cassette insertion
NHAPC5	GABPB1L-2	3	1	Puro cassette insertion	13bp frameshift deletion + G>T sub
NHAPC5	GABPB1L-2	2	2	Puro cassette insertion	4bp frameshift deletion

Parental	sgRNA	GABPB1L copy number	Clone #	GABPB1L allele 3	GABPB1L allele 4	GABPB1L allele 5
GBM1	GABPB1L-1	2	1			
GBM1	GABPB1L-2	2	2			
T98G	GABPB1L-2	5	1	7bp frameshift deletion + A>T sub	3bp in-frame deletion	7bp frameshift deletion + A>G sub
T98G	GABPB1L-2	5	2	13bp frameshift deletion + G>A sub	3bp in-frame deletion	13bp frameshift deletion
LN229	GABPB1L-2	3	1	Wild-type		
LN229	GABPB1L-2	3	2	5bp frameshift deletion		
HCT116	GABPB1L-2	2	1			
HCT116	GABPB1L-2	2	2			
HEK293T	GABPB1L-2	3	1	Wild-type		
HEK293T	GABPB1L-2	4	2	7bp frameshift deletion	3 bp-inframe deletion	
NHAPC5	GABPB1L-2	3	1	14bp frameshift deletion + TGA>GTT trinucleotide sub		
NHAPC5	GABPB1L-2	2	2			

Table S3, related to Figure 2. Deletions induced by site-directed mutagenesis for the NanoBiT Protein-Protein Interaction assay.

Deletion	Deletion	Forward Primer	Reverse Primer
Reference	CAGCTCCTAAAGA AAGAACAGGAAG CAGAGGCCTACA GACAGAAGT	N/A	N/A
DEL1	CAGCTCCTAAAGA ---AACAGGAAGCA GAGGCCTACAGA CAGAAG	GCCTCTGCTTCCT GTTTCTTTAGGAG CTGCTGT	ACAGCAGCTCCT AAAGAAACAGGA AGCAGAGGC
DEL2	CAGCTCCTAAAGA AAGAACAGGAAG CAGAGGCCTACA GAC---AG	GCAGAGGCCTAC AGACAGTTGGAA GCTATGAC	GTCATAGCTTCC AACTGTCTGTAG GCCTCTGC
DEL3	CAGCTCCTAAAGA AAGAACAGGAAG CAGTGGCCTAC--- ----AG	GTCATAGCTTCCA ACTGTAGGCCTCT GCTTCC	GGAAGCAGAGG CCTACAGTTGGA AGCTATGAC

Table S4, related to Figure 3. EdgeR output for RNA-seq differential expression analysis – significantly dysregulated transcripts.

Gene	logFC	logCPM	p value	FDR	GABP
HDC	8.049086875	1.534769377	3.77E-06	1.19E-06	TRUE
MT1L	-7.989910871	-0.09863883	2.44E-05	1.26E-06	FALSE
NTRK2	-3.801031266	5.058510457	6.89E-06	2.54E-06	TRUE
TMEM176A	-7.828825804	0.439729758	9.22E-06	4.19E-06	TRUE
TFPI2	-2.874635985	7.834920197	8.71E-05	8.17E-06	TRUE
ZP4	-6.734234171	0.813997408	0.00013234	2.08E-05	TRUE
PI15	-5.251817299	6.838739379	0.000173299	2.72E-05	FALSE
HGF	-5.780473372	6.411448335	0.000182063	4.11E-05	TRUE
A2M	-3.90727389	3.235761001	0.000191627	6.11E-05	TRUE
CNTN4	-4.973501689	-0.134486213	0.000197853	8.29E-05	FALSE
MUC15	-6.463653621	-1.409534524	0.000318064	8.60E-05	TRUE
TMEM176B	-6.349304655	0.512662696	0.00011121	9.35E-05	TRUE
PAQR5	-4.491424719	1.761862136	0.000357144	9.75E-05	TRUE
S100A8	-6.773080973	-2.084263094	0.0006697	1.29E-04	TRUE
MTTP	-4.278526143	0.639690227	0.000694093	2.25E-04	FALSE
CXCL5	-6.837437146	3.362177431	0.00084337	5.73E-04	TRUE
PRSS35	-3.677812557	0.831253062	0.001034112	9.17E-04	TRUE
TACR1	-4.73275274	1.792163114	0.001269826	1.07E-03	TRUE
VWA5A	-2.738634399	3.818059734	0.001277974	1.41E-03	TRUE
TSLP	-3.797641961	3.815510008	0.001441245	1.60E-03	TRUE
MUC5AC	-5.126047524	-2.303393351	0.001500022	1.86E-03	TRUE
CCL8	-5.717612815	-2.736059689	0.001518843	1.96E-03	FALSE
CFTR	-3.825218875	-0.600083635	0.001760891	2.20E-03	TRUE
GPR183	-3.874628273	0.61338171	0.001785725	2.23E-03	FALSE
SCUBE1	-3.849578634	3.312764199	0.002940318	2.32E-03	TRUE
FILIP1L	-1.848658792	5.016795205	0.003072085	3.10E-03	TRUE
UGT1A1	-3.561228945	1.893582292	0.004333414	3.34E-03	TRUE
MTHFD2P1	-3.561633667	-1.758630997	0.004428382	3.51E-03	FALSE
UGT1A8	-3.518566387	1.591617307	0.004566677	3.63E-03	FALSE
UGT1A9	-3.538689569	1.59770364	0.004577247	4.17E-03	TRUE
UGT1A10	-3.504242342	1.700953281	0.004685119	4.18E-03	FALSE
UGT1A5	-3.525442375	1.58501437	0.004776638	4.28E-03	FALSE
EDNRB	-2.261135408	2.865627923	0.014262394	0.004444416	FALSE
NPBWR1	-3.977255085	-1.108536696	0.014850829	0.00445532	TRUE
ADAMTS19	-4.734767573	0.56944742	0.015181039	0.004478805	FALSE
OSM	-4.095304118	-2.869050941	0.015328682	0.004498565	TRUE
FERMT3	4.059645569	2.634903971	0.016129071	0.004509658	TRUE
COMP	5.503876556	0.978430995	0.0164529	0.004594366	TRUE

Gene	logFC	logCPM	p value	FDR	GABP
HOXC12	-3.208929659	-0.224485887	0.016653143	0.004627978	FALSE
TINCR	-2.61118365	-0.134312744	0.017025472	0.004653365	TRUE
CPXM2	7.197628142	-0.966334184	0.017044629	0.004821912	TRUE
DRD2	-1.949115207	3.748832303	0.004809774	4.86E-03	TRUE
ABCB1	-2.433482964	2.224454507	0.017065987	0.004909037	FALSE
TRIML2	4.550835773	1.722655111	0.017336914	0.004969468	FALSE
UGT1A4	-3.511937281	1.596721156	0.00491148	4.99E-03	FALSE
S100A9	-3.91784833	-2.672701298	0.017457842	0.00516369	FALSE
TP63	-3.097465443	0.319658804	0.00492949	5.23E-03	TRUE
VNN2	-3.027144065	-0.538213922	0.018570754	0.005292244	FALSE
UGT1A3	-3.495685058	1.589368931	0.005137623	5.33E-03	TRUE
GFRA2	-3.354650807	-0.749213654	0.019250326	0.00544878	TRUE
C22orf46	-1.03814487	5.076260978	0.01930086	0.005467721	TRUE
GABRG3	7.085237061	-1.031518934	0.019352297	0.005476896	TRUE
KCNJ10	-2.571389807	2.346726925	0.00513901	5.59E-03	TRUE
CCDC129	-3.615719758	-1.53000084	0.019598041	0.005614059	FALSE
ARHGAP25	-3.486817326	0.242890108	0.005234542	5.77E-03	TRUE
UGT1A7	-3.447066763	1.640343407	0.005304868	0.005848268	FALSE
LGI4	-3.790906923	0.761719472	0.00560607	0.006007118	TRUE
TEK	-3.015645979	1.01637584	0.00738532	0.006060308	FALSE
ITGA9	-3.559080425	3.60719519	0.007523789	0.006083852	FALSE
STX11	2.646991911	-0.765271846	0.021178821	0.006195461	TRUE
UGT1A6	-3.277894992	1.648205951	0.007620153	0.006674252	TRUE
SLFN11	-3.178072399	2.584142303	0.008305631	0.006708686	FALSE
CARD11	7.308911168	-0.838862701	0.021942509	0.006723478	FALSE
DKK1	1.135862979	6.399609258	0.022161744	0.006946396	TRUE
GCSAML	6.874139498	0.522575017	0.022162054	0.006974946	FALSE
CALB2	-2.274708124	1.739600397	0.022303459	0.007561587	TRUE
CFAP221	-2.990164784	-2.596804459	0.02245537	0.007823833	TRUE
ICK	-1.177529362	5.897133924	0.022716856	0.007890192	TRUE
THNSL2	-3.16747966	-0.972890533	0.023300243	0.008007116	TRUE
COL9A1	-2.742505255	-1.714713086	0.023681437	0.008038152	TRUE
TRPM2-AS	-4.395247768	-2.10122456	0.008537099	0.008051612	FALSE
LINC01133	5.831857229	-2.052404013	0.024068601	0.008079827	FALSE
MPZ	-2.631848196	3.451720212	0.024437679	0.008124566	TRUE
HEPH	4.310881045	3.728269252	0.024505373	0.008259386	FALSE
LRP5	1.04218618	5.732934467	0.024530521	0.008376253	TRUE
HCN4	6.206765563	-1.749480676	0.008568601	0.008520386	FALSE
CXCL8	-2.288300058	7.285245286	0.024680431	0.008756094	FALSE
GABRA4	-3.886309225	-2.31045504	0.024697297	0.008860847	FALSE

Gene	logFC	logCPM	p value	FDR	GABP
MGP	-1.920748301	2.375862658	0.024801536	0.008928433	FALSE
OGN	6.692662816	-1.361769578	0.024813785	0.008988919	FALSE
RPS6KA6	-3.760920498	-0.288239957	0.008742063	0.00900248	FALSE
CXCR4	-3.700241393	-1.305420529	0.009008515	0.009339566	TRUE
NPY	-4.379119282	-2.092551971	0.009180153	0.009351572	TRUE
LBH	2.105996896	4.635818061	0.025395215	0.009365974	TRUE
SEMA3D	-2.222618065	3.833299548	0.025509284	0.009493437	FALSE
GLI2	1.393347145	4.996311567	0.025587327	0.009545176	TRUE
TUBA3C	8.571782441	0.305583691	0.025886545	0.009702786	FALSE
CXCL6	-5.012642468	1.653448556	0.009901244	0.009815216	FALSE
PNOC	6.260495697	-0.073299604	0.025945077	0.009897571	TRUE
FGF7	-2.477426869	3.972114776	0.010624697	0.009924656	FALSE
FAM201A	-3.515216991	-1.824509379	0.026263397	0.009956998	TRUE
STC1	-2.180908534	7.999952952	0.011066431	0.010564754	TRUE
GSTM5	-2.503638212	-2.172205278	0.02767625	0.010803378	TRUE
RHOU	-1.98871111	2.688956941	0.027822359	0.010889103	TRUE
ICAM1	-2.019958711	4.131686188	0.028481383	0.011091675	TRUE
CAMK2N1	1.364850862	6.223506183	0.028697019	0.011303897	TRUE
ANO4	-3.484510206	1.666359696	0.011428259	0.011408738	FALSE
LAMP3	-3.552223597	-1.075469772	0.011445934	0.011553314	FALSE
RASSF6	-3.064589784	-0.776612714	0.028959196	0.011587878	TRUE
EDIL3	-1.317223734	6.688413125	0.011531743	0.011705774	FALSE
LGSN	-3.69178738	-2.747318921	0.029043535	0.011921747	TRUE
CCR3	-3.093616007	-1.921380037	0.029670965	0.012367675	FALSE
LPAR3	-3.227301426	-2.701511134	0.030266733	0.013052732	FALSE
CELF2	-2.041409873	3.80630249	0.030985932	0.013071533	TRUE
LINC01915	-3.375066359	0.336963229	0.011647698	0.013447724	FALSE
MMP10	-2.904323636	-1.33229792	0.031065334	0.013849581	FALSE
C19orf81	5.604702183	-2.202590718	0.031431958	0.013868809	TRUE
MAGEB6	3.498881725	-0.411480195	0.031494237	0.013904022	FALSE
SHANK1	4.099124742	1.03358378	0.031765229	0.014038482	FALSE
ADD2	3.494912278	5.038973012	0.012322207	0.014135468	TRUE
CEMIP	1.793909161	5.140891621	0.032585671	0.014406602	TRUE
CA8	-2.754297386	1.669390029	0.013297412	0.014572724	TRUE
ANKRD1	3.070558745	1.945731811	0.013434979	0.014815634	TRUE
RCSD1	-3.035952408	-1.333739678	0.013506384	0.014916236	TRUE
RARRES2	-2.991917543	0.725467047	0.033119001	0.014958541	TRUE
FAR2P2	-3.345728563	-1.97643088	0.033209553	0.015243021	FALSE
KRTAP2-3	2.667296044	0.124150413	0.033413427	0.0156409	FALSE
CP	3.321487346	3.428477829	0.033423621	0.015735756	TRUE

Gene	logFC	logCPM	p value	FDR	GABP
TMEM100	-2.033055064	4.333255512	0.033511783	0.017176861	TRUE
EPHB6	4.240470791	0.070251498	0.033641561	0.017564371	FALSE
ADAMTS2	2.380152602	4.706452222	0.034311407	0.017650344	TRUE
IL32	2.274203801	2.225854337	0.034977936	0.017810539	FALSE
TERT	-1.750307861	0.213014433	0.035226626	0.017823031	TRUE
VNN1	-2.756717353	-0.088878982	0.03586095	0.018046593	FALSE
PIEZO2	-2.256951639	5.926920198	0.035915145	0.018708996	TRUE
FST	-1.330299012	4.259125321	0.036245576	0.019504434	FALSE
MMP13	-3.40515214	4.267422058	0.036613208	0.020313136	FALSE
CUZD1	3.371428711	-0.134743191	0.036793542	0.02035303	FALSE
SYTL2	-1.245575095	6.001499744	0.03706273	0.02088963	TRUE
MAGEA10	6.028351547	-0.258151211	0.037168142	0.021329389	FALSE
DCT	-2.565663132	-1.442067073	0.037819313	0.021565603	TRUE
CPA6	-2.620437648	-0.545367347	0.037839646	0.021955062	FALSE
ZNF853	-2.231638703	2.135426603	0.037874743	0.022444453	TRUE
OBSCN	1.669276202	4.645274953	0.03794602	0.023967613	TRUE
SOD3	-3.352493857	4.218582864	0.038036124	0.024124595	FALSE
NTF3	3.721204024	1.922630691	0.038242526	0.024377605	TRUE
ITIH6	-3.957590458	0.909436366	0.038347785	0.025953053	FALSE
RASGRP3	-1.636705793	4.04621766	0.038583385	0.026088634	FALSE
ZDHHC15	-2.414043718	-1.293863375	0.038633607	0.026574069	FALSE
SLC27A2	7.048488564	-1.099868085	0.039556893	0.027863375	FALSE
GABPB1	0.958566168	5.287148867	0.040974398	0.028450711	TRUE
PRG4	5.131122265	1.44118635	0.041760287	0.028461106	FALSE
INPP4B	1.156260342	4.794478797	0.042015845	0.028539707	TRUE
TRBC2	6.319154779	0.764636991	0.0428078	0.028948732	FALSE
PTPRO	3.093470433	0.042944827	0.043106557	0.029129824	FALSE
DHRS2	2.458361885	3.316124571	0.043208714	0.029242938	TRUE
PCDH17	-1.867341817	1.770862128	0.043232785	0.029407116	FALSE
FRK	-1.763423284	2.147253479	0.043593579	0.029459898	TRUE
GNAI1	-1.00740864	5.872330238	0.044810868	0.029862901	TRUE
PCOLCE	0.99487556	7.685532591	0.045121619	0.030036488	TRUE
CD1D	4.303185934	0.402900161	0.045846003	0.03181145	FALSE
OLMALINC	-1.722715746	2.635640775	0.046590009	0.032586978	FALSE
ARHGEF35	-2.67250947	-0.847504702	0.04681797	0.033781237	FALSE
AKR1B1	-1.050628598	8.161878847	0.047029972	0.03402702	FALSE
IL1B	-2.434407874	4.330995301	0.047723229	0.035596027	TRUE
PTGS2	-1.832849526	4.098331802	0.048697998	0.03585096	TRUE
DEFB124	-3.375675068	-1.280762949	0.048851133	0.041407851	FALSE
TF	-2.284190047	3.960297857	0.049367378	0.04703088	TRUE

Table S5, related to Figure 3. GO-enrichment for genes differentially expressed between control and GABPβ1L-reduced *TERT* promoter mutant lines.

Process	GOTerm Accession	Gene Determinants	FDR
Glucuronidation	0052697	UGT1A10, UGT1A8, UGT1A1, UGT1A4, UGT1A5, UGT1A3, UGT1A9	1.44E-11
	1904223		
	1904224		
	2001030		
	2001029		
	0052696		
	0052695		
	0006063		
	0019585		
Cellular development	0044707	HOXC12, RHOU, FST, COL9A1, TMEM176B, SHANK1, UGT1A1, LRP5, EDIL3, CXCR4, NTF3, NPY, OGN, DKK1, GPR183, ZDHHC15, LGI4, RPS6KA6, ICK, FRK, MGP, LPAR3, ADAMTS2, KCNJ10, FERMT3, SP7, TERT, S100A9, VNN1, NTRK2, GABRA4, STC1, S100A8, PCOLCE, CD1D, PTGS2, KCNA1, ANKRD1, HGF	3.0903E-08
	0044767		
	0032502		
	0044763		
	0048856		
	0048869		
	007275		
Cell-to-cell signaling	0007267	STX11, DKK1, LPAR3, TACR1, HCN4, KCNJ10, NPBWR1, SHANK1, TERT, S100A9, NTRK2, CXCL5, GABRA4, LRP5, CCL8, PTGS2, KCNA1, NTF3, NPY, HGF	8.26038E-08
	0099536		
	0099537		

Process	GoTerm Accession	Gene Determinants	FDR
Fatty acid metabolism	0045922	UGT1A10, UGT1A8, UGT1A1, UGT1A4, UGT1A3, UGT1A9	8.31764E-07
	0019217		
	0045833		
Cell differentiation	0030154	DKK1, FST, GPR183, LGI4, FRK, MGP, COL9A1, LPAR3, TMEM176B, KCNJ10, FERMT3, SP7, SHANK1, VNN1, S100A9, NTRK2, STC1, LRP5, CXCR4, S100A8, CD1D, PTGS2, KCNA1, NTF3, NPY, OGN, HGF, ANKRD1	2.58226E-07
Cell proliferation	0008283	GPR183, LGI4, FRK, TACR1, ABCB1, ZP4, TERT, NTRK2, CXCL5, STC1, LRP5, CCL8, CD1D, PTGS2, KCNA1, NPY, NTF3, HGF, OGN	8.29851E-06

CHAPTER 3: DISRUPTION OF GABPβ1L FUNCTION IS SUFFICIENT TO REVERSE GLIOBLASTOMA REPLICATIVE IMMORTALITY IN A *TERT* PROMOTER MUTATION-DEPENDENT MANNER

3.1 ABSTRACT

The ETS family transcription factor GABP binds to and activates the mutant *TERT* promoter as a GABPβ1L-containing GABP tetramer in glioblastoma. Using CRISPR-Cas9-mediated disruption of GABPβ1L function in glioblastoma, we have identified GABPβ1L as necessary for cellular immortality in a *TERT* promoter mutation-dependent manner. Reduction in GABPβ1L function was sufficient to induce telomere shortening and loss of cellular viability exclusively in *TERT* promoter mutant glioblastoma lines *in vitro*. Expression of exogenous GABPβ1L or TERT was sufficient to fully and immediately rescue both telomere shortening and cell death phenotypes. Additionally, orthotopic xenografting of GABPβ1L-reduced, *TERT* promoter mutant glioblastoma cells rendered lower tumor burden and longer overall survival in mice. These results highlight the critical role of GABPβ1L in enabling immortality in *TERT* promoter mutant glioblastoma.

3.2 GABPβ1L-MEDIATED ACTIVATION OF THE MUTANT *TERT* PROMOTER IS REQUIRED FOR TELOMERE MAINTENANCE IN GBM

As *TERT* expression is closely linked to telomere maintenance, we next investigated the effects of reducing GABPβ1L function on telomere length in the *TERT* promoter mutant cell lines. Measurements of mean telomere length at four time points following editing uncovered significant telomere loss only in clones from *TERT* promoter mutant cells with reduced GABPβ1L function (Figure 4A). Expression of exogenous GABPβ1L or TERT was sufficient to halt this telomere loss in all clones (Figure 4B). Telomere shortening and uncapping can result in end-to-end fusions of telomere-deficient chromosomes and the formation of chromatin bridges (Capper et al., 2007; der-Sarkissian et al., 2004; Hackett et al., 2001). We identified chromatin bridges in a significant proportion of the *TERT* promoter mutant, but not *TERT* promoter wild-type, GABPβ1L-reduced clones 70-75 days after editing, indicating widespread telomere dysfunction following telomere loss (Figures 4C and S4A). Telomere dysfunction was readily rescued by expression of exogenous GABPβ1L or TERT (Figures S4B and S4C). These data support that disrupting GABPβ1L function is sufficient to induce telomere loss and dysfunction in a *TERT* promoter mutation-dependent manner.

3.3 DISRUPTING GABPβ1L FUNCTION IS SUFFICIENT TO INDUCE SHORT-TERM AND LONG-TERM GROWTH DEFECTS IN *TERT* PROMOTER MUTANT LINES *IN VITRO*

Previous studies have reported that *TERT* depletion and telomere dysfunction result in both immediate and long-term growth defects (Cao et al., 2002; Fitzgerald et

al., 1999; Iwado et al., 2007; Shay and Wright, 2006). Thus we sought to determine whether reduction of GABPβ1L results in a growth phenotype as a result of reduced expression from the mutant *TERT* promoter. Monitoring cell growth prior to significant telomere loss (days 45-48 post-editing) revealed a growth defect in all *TERT* promoter-mutant GABPβ1L-reduced clones (Figure S5A). We further inhibited β1L in the β1L-reduced lines with an LNA-ASO to deplete any residual β1L function and observed no further changes in cell growth (Figure S5B) or *TERT* expression (Figure S5C) regardless of *TERT* promoter status. Interestingly, LNA-ASO-mediated knockdown of GABPβ1L in *TERT* promoter mutant control lines significantly reduced cell growth compared to the LNA-ASO controls, suggesting a short-term growth effect following reduction of GABPβ1L and TERT levels.

Long-term changes in growth and cell viability may occur due to telomere dysfunction in the *TERT* promoter mutant, GABPβ1L-reduced clones. We monitored each GABPβ1L-reduced line throughout the process of telomere loss and identified a progressive loss of cell viability in GABPβ1L-reduced clones from *TERT* promoter mutant cells, a phenotype that was absent in the clones from *TERT* promoter wild-type cells (Figure 5A). We observed complete growth arrest in both GBM1 GABPβ1L-reduced clones, and substantial but incomplete arrest of the cultures of T98G and LN229 clones. GABPβ1L-reduced clones derived from T98G underwent complete growth arrest in all cases except one instance when a surviving population emerged following long-term culture. Unlike GBM1 and T98G cells, both LN229 clones consistently had a population of viable cells emerge following the period of massive cell death. The underlying cause of this heterogeneity in cellular response among the three

lines is unknown, but could reflect residual function of GABPβ1L in GABPβ1L-reduced clones, potential GABPβ1L-independent mechanisms of activation of the mutant *TERT* promoter, or other factors. Importantly, overexpression of either exogenous GABPβ1L or TERT was sufficient to counteract the loss of viability (Figure 5B). This gradual loss of viability signified the loss of replicative immortality in *TERT* promoter mutant GABPβ1L-reduced clones.

3.4 GABPβ1L-REDUCED GBM LINES ACCRUE DNA DAMAGE AND UNDERGO MITOTIC CELL DEATH IN A *TERT* PROMOTER MUTATION-DEPENDENT MANNER

The direct correlation between telomere shortening and viability loss (Figure S6A) suggested that the loss of viability is a consequence of cell death or senescence induced by telomere dysfunction. The formation of chromatin bridges after telomere dysfunction induces breakage-fusion-bridge cycles that lead to the accrual of significant DNA damage in telomere-deficient cells (der-Sarkissian et al., 2004; Hackett et al., 2001). While canonical apoptosis and cellular senescence have been widely observed as results of significant DNA damage after telomere dysfunction, both mechanisms are dependent on functional p53 and RB pathways (Saretzki et al., 1999; Whitaker et al., 1995). However, these two pathways are commonly mutated in *TERT* promoter mutant GBM, including the GBM1, T98G, and LN229 lines (Table S6), making apoptosis and senescence unlikely to occur at high levels. In p53- and RB-deficient cells, mitotic cell death has been implicated as a primary phenotype following telomere dysfunction (Fragkos and Beard, 2011; Hayashi et al., 2015). Mitotic cell death can result from chromosome fusions, high-level chromosomal rearrangements and DNA damage, oft-

described consequences of breakage-fusion-bridge cycles during telomere dysfunction (Hayashi et al., 2015; Vakifahmetoglu et al., 2008; Vitale et al., 2011).

Indeed, we observed a significant increase in the amount of the DNA damage marker γ-H2AX exclusive to the GABPβ1L-reduced clones from *TERT* promoter mutant cells by day 73 post- editing (Figures 6A and S6B). Likewise, we identified giant cell micronucleation, a prominent feature of mitotic cell death (Ianzini and Mackey, 1997; Vakifahmetoglu et al., 2008), in GABPβ1L-reduced, *TERT* promoter mutant – but not wild-type – cells at this same time point (Figures 6B and S6C). Overexpression of exogenous GABPβ1L or TERT was sufficient to fully rescue both the DNA damage (Figure S7A) and mitotic cell death phenotypes (Figure S7B). Additionally, chromatin bridge formation, γ-H2AX staining, and giant cell micronucleation accumulated over three time points (days 45, 61, and 73 post-editing) in the LN229 β1L-reduced clones, thus supporting that these phenotypes may be dependent on telomere shortening (Figure S7C).

Moreover, cell cycle analysis of the GABPβ1L-reduced *TERT* promoter mutant cells between day 70 and day 80 post-CRISPR-Cas9 editing revealed a modest G_2/M enrichment, another hallmark of cells undergoing mitotic cell death (Deeraksa et al., 2013) (Figures 6C and 6D). Cytometric analysis of senescence and apoptosis/necrosis markers identified a modest increase in apoptosis in *TERT* promoter mutant GABPβ1L-reduced clones, thereby implicating non-apoptotic mitotic cell death, with modest contributions from canonical apoptosis, as the primary driver of cell death in these lines (Figure S7D). Therefore, *TERT* promoter mutation-dependent telomere dysfunction induced by reducing the function of the GABP tetramer-forming isoform GABPβ1L and

reducing *TERT* expression culminates in a loss of replicative immortality characterized by a profound loss of cell viability primarily driven by a mitotic cell death mechanism.

3.5 REDUCING GABPβ1L FUNCTION IMPAIRS TUMOR GROWTH AND EXTENDS MOUSE SURVIVAL *IN VIVO*

In order to determine the effects of GABPβ1L disruption in a *TERT* promoter mutant setting *in vivo*, we orthotopically injected CRISPR control or GABPβ1L-reduced LN229 cells expressing luciferase into nude mice and monitored tumor engraftment and growth via bioluminescence imaging (BLI). A proportion of the mice injected with GABPβ1L-reduced tumor cells did not show evidence of tumor formation over the time course, and those that did form tumors showed significantly decreased tumor growth when compared to mice injected with control cells (Figures 7A and 7B). Importantly, mice injected with the control lines had a significantly shorter median survival compared to mice bearing the β1L-reduced lines (Figure 7C). Despite LN229 C1 and C2 having an attenuated growth arrest phenotype compared to the other lines (Figure 5A), GABPβ1L disruption and reduced *TERT* expression in these lines were sufficient to significantly inhibit tumor formation and growth and extend survival in mice injected with them. Furthermore, lentiviral transduction of LN229 C1 and C2 with a TERT expression vector was sufficient to rescue both the tumor growth and survival phenotypes (Figures 7D-F). In conclusion, inhibition of the mutant *TERT* promoter through disrupting GABPβ1L function is sufficient to prolong survival in mice bearing GBM xenografts.

3.6 MAIN FIGURES

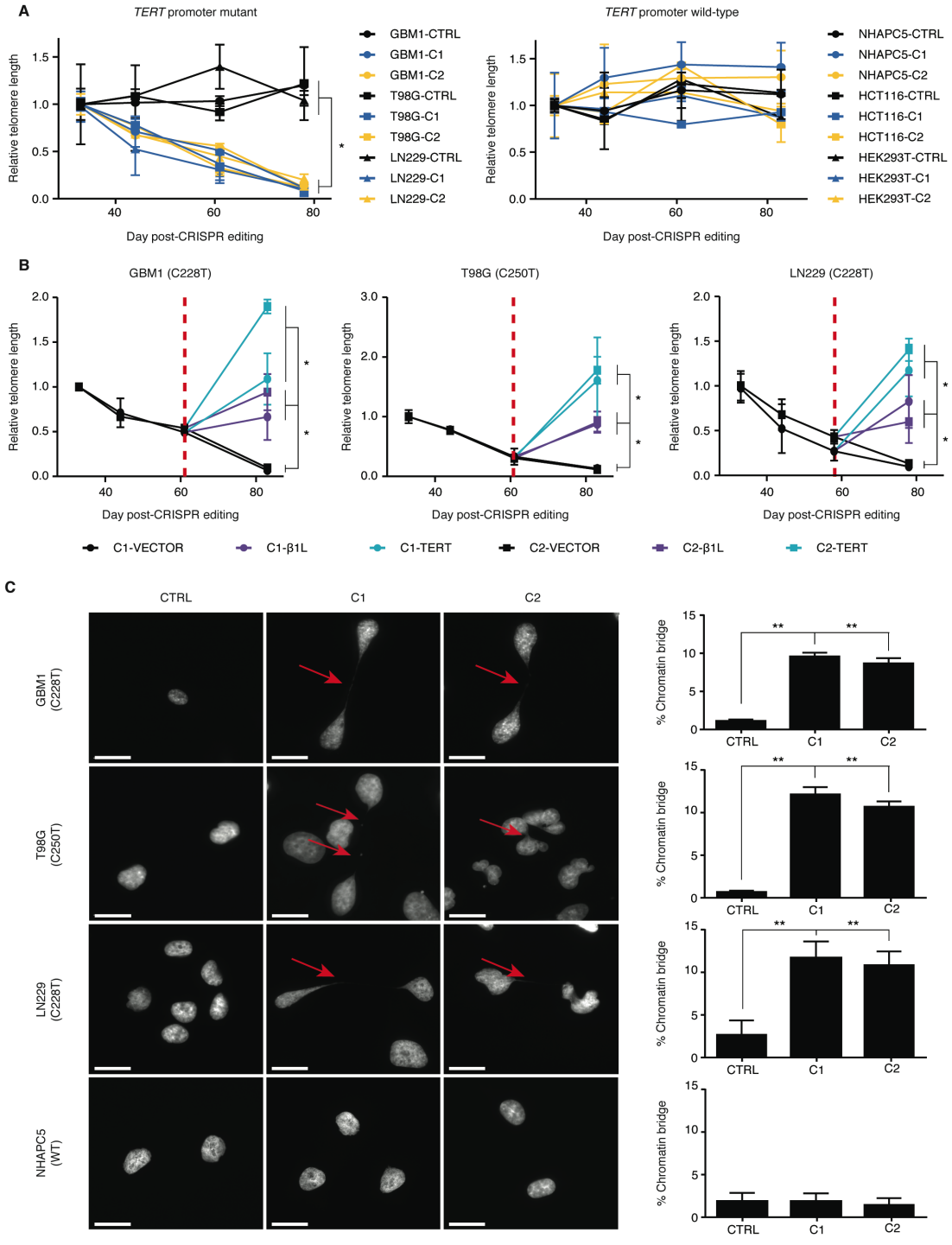

Figure 4. GABPβ1L-mediated activation of the mutant *TERT* promoter is required for telomere maintenance in GBM.

(A) Telomere length at days 44, 61, and 78 in *TERT* promoter mutant lines or days 44, 61 and 83 in *TERT* promoter wild-type lines post-editing relative to day 33 post-editing

for CTRL or GABPβ1L-reduced clones. *p value<0.05, two-sided Student's t-test comparing values between CTRL and GABPβ1L-reduced clones at day 78/83 for each respective line. Values are mean ± S.D. of at least three independent assays.
(B) Relative telomere length after transfection of an empty (VECTOR), GABPβ1L, or TERT expression vector in *TERT* promoter-mutant lines 78 or 83 days post-editing. Red dotted line indicates time of transfection (at day 58 [LN229] or 61 [GBM1 and T98G] post-editing). *p value<0.05, two-sided Student's t-test of values of GABPβ1L or TERT versus VECTOR at day 78/83. Values are mean ± S.D. of at least three independent experiments.
(C) Representative DAPI images (left images) and quantification (right graphs) of chromatin bridges (arrow) in CTRL or GABPβ1L-reduced clones at days 70-75 post-editing. Scale bar = 20 μm. *p value<0.05, **p value<0.01, two-sided Student's t-test compared to CTRL. Quantification values are weighted mean ± S.D. of at least ten independent fields of view.
See also Figure S4.

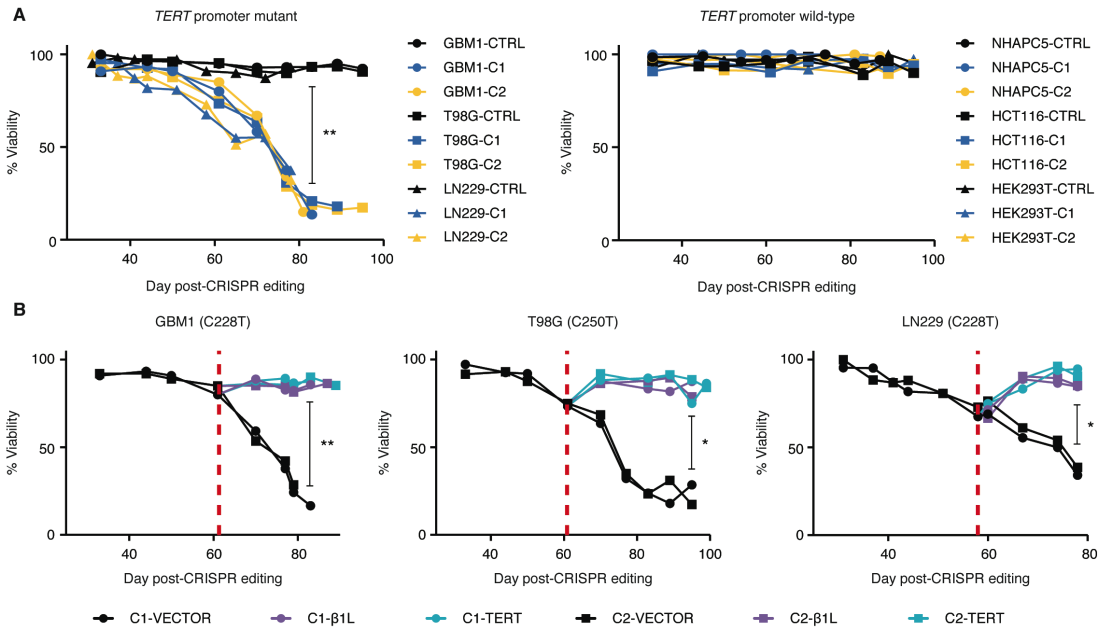

Figure 5. GABPβ1L reduction induces loss of replicative immortality in *TERT* promoter-mutant GBM lines.

(A) Cell viability of CTRL or GABPβ1L-reduced clones measured approximately every 7 days from day 33 to day 99 post-editing for *TERT* promoter mutant and wild-type lines. **p value<0.01, Welch's t-test of CTRL clones versus GABPβ1L-reduced clones at day 83 post-editing.

(B) Cell viability measurements following transfection with an empty (VECTOR), GABPβ1L, or TERT expression vector. Red dotted line indicates time of transfection. *p value<0.05, **p value<0.01, Welch's t-test of vector transfected cells versus GABPβ1L and TERT transfected cells at the final recorded time-point for each line.

Values are median of three independent experiments.

See also Figure S5.

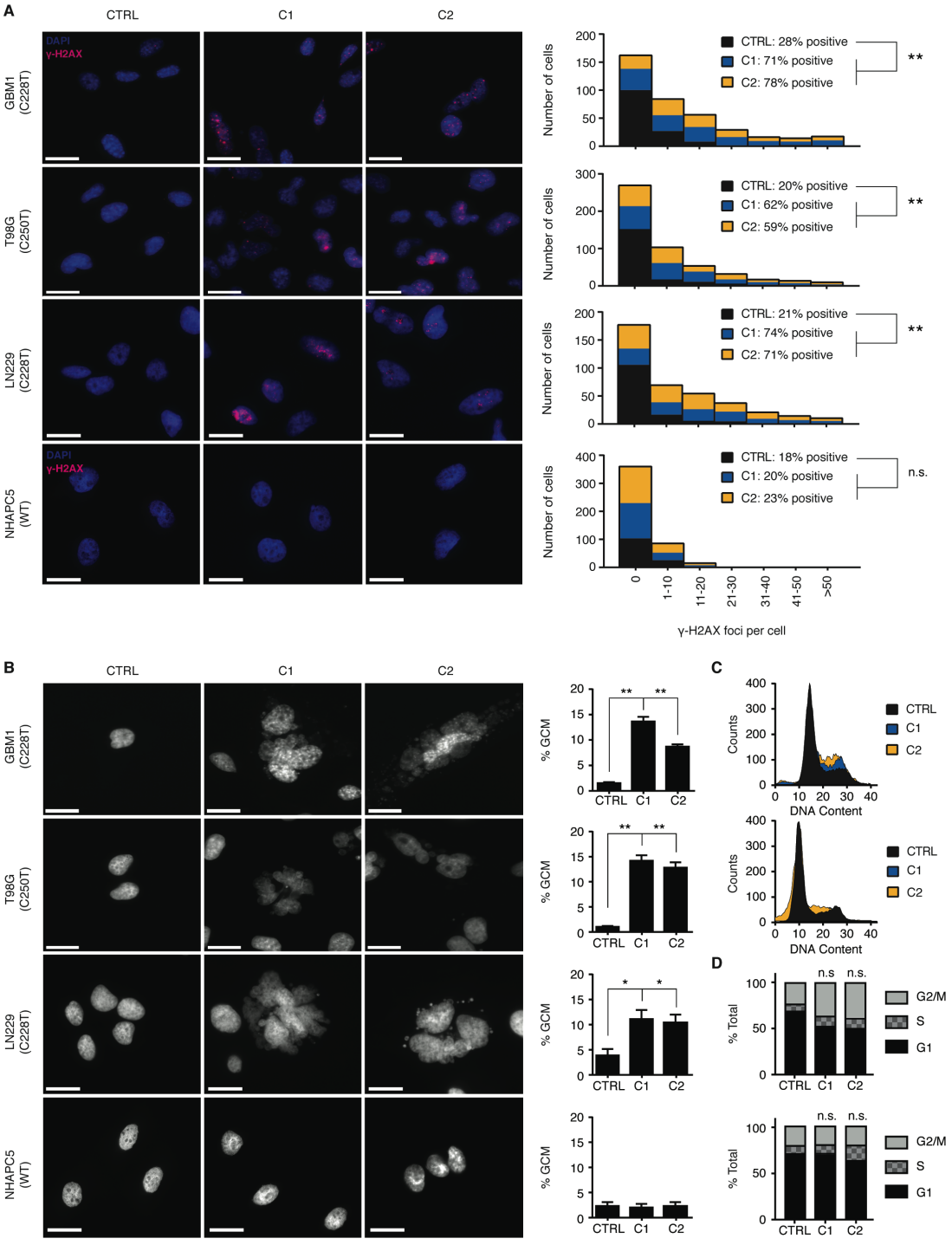

Figure 6. GABPβ1L-reduced GBM lines accrue DNA damage and undergo mitotic cell death in a *TERT* promoter mutation-dependent manner.

(A) Representative images (left images) and quantification (right graphs) of γ-H2AX staining in CTRL or GABPβ1L-reduced clones at day 70-75 post-editing. Scale bar =

20µm. **p value<0.01, two-sided Student's t-test compared to CTRL. Quantification values are sums of at least ten independent fields of view.
(B) Representative DAPI images (left images) and quantification (right graphs) of giant cell micronucleation (GCM) in CTRL or GABPβ1L-reduced clones at day 70-75 post-editing. Scale bar = 20 µm. *p value<0.05, **p value<0.01, two-sided Student's t-test compared to CTRL. Quantification values are weighted mean ± S.D. of at least ten independent fields of view.
(C,D) Histograms **(C)** and quantification **(D)** for cell cycle analysis of CTRL or GABPβ1L-reduced LN229 (top graphs) and NHAPC5 (bottom graphs) lines at day 75 post-editing.
See also Figures S6-S7 and Table S6.

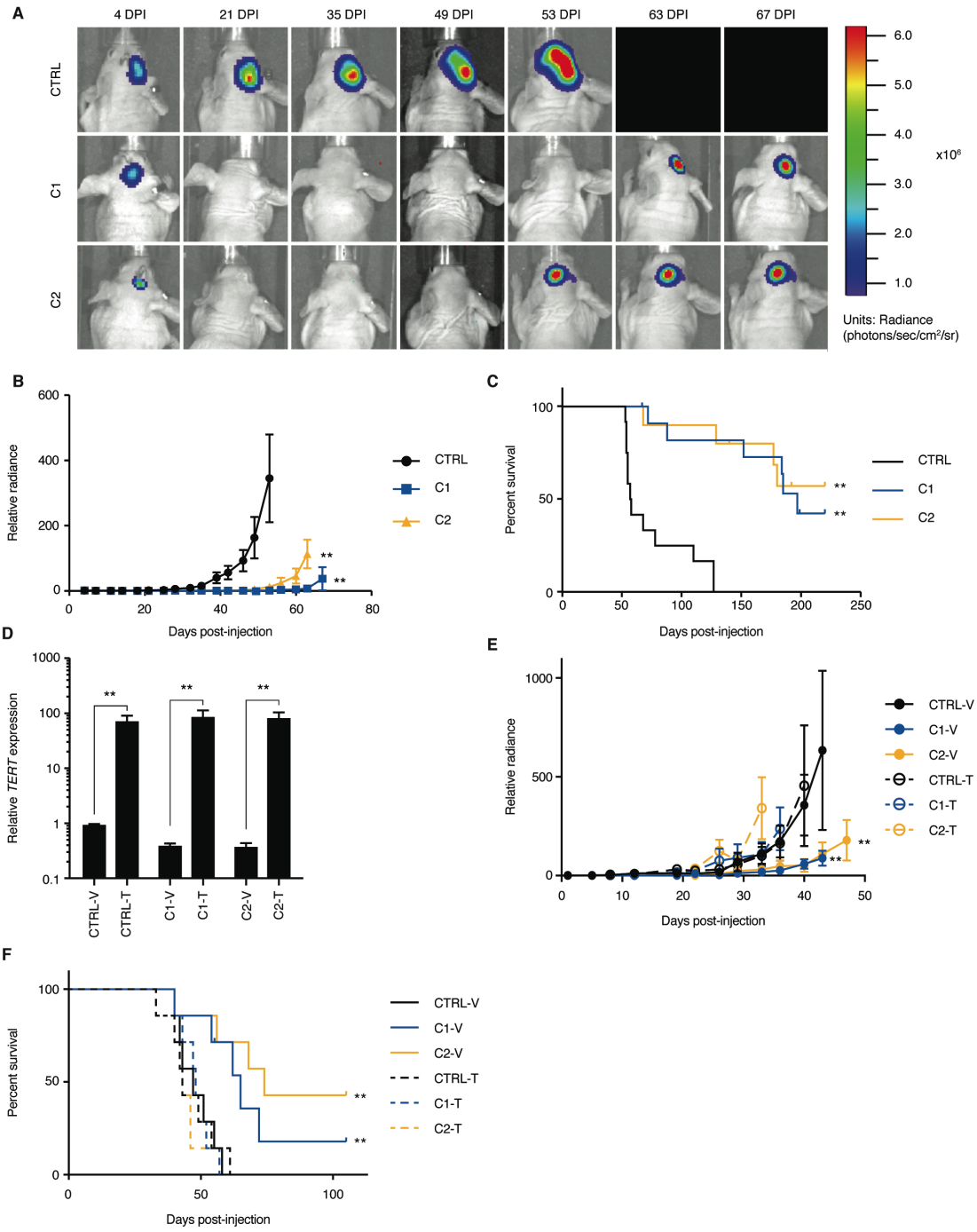

Figure 7. Reduction of GABPβ1L impairs tumor growth and extends mouse survival *in vivo*.

(A) Representative IVIS bioluminescent images of CTRL or GABPβ1L-reduced LN229-derived tumors at 7 time points post-intracranial injection (injected on cellular day 51 post-editing). DPI = days post-injection.

(B) Relative tumor bioluminescence quantified twice per week for each group (CTRL: n=12, C1: n=12, C2: n=10) until first recorded mortality. **p value<0.01, two-sided Student's t-test compared to CTRL peak luminescence. Values are mean ± S.D of all mice in each group.
(C) Kaplan-Meier survival curve displaying disease-specific survival of mice (Simonsen Labs) injected with LN229 CTRL or C1 and C2 GABPβ1L-reduced cells over time. **p value<0.01, log-rank test compared to CTRL.
(D) *TERT* expression 4 days post-transduction of CTRL or GABPβ1L-reduced LN229 clones (41 days post-editing) with either a control (V) or TERT (T) lentiviral expression vector. **p value<0.01, two-sided Student's t-test relative to respective vector (V) control. Values are mean ± S.D of three independent experiments**.**
(E) Relative tumor bioluminescence quantified twice per week for each group (n=7 mice per group) following stable transduction with a control (V) or TERT (T) lentiviral expression vector. **p value<0.01, two-sided Student's t-test compared to vector control peak luminescence for each respective line. Values are mean ± S.D of all mice in each group.
(F) Kaplan-Meier survival curve displaying disease-specific survival of mice (Envigo) injected with LN229 CTRL or C1 and C2 GABPβ1L-reduced cells following stable transduction with a control (V) or TERT (T) lentiviral expression vector. **p value<0.01, log-rank test compared to CTRL.

3.7 SUPPLEMENTAL FIGURES

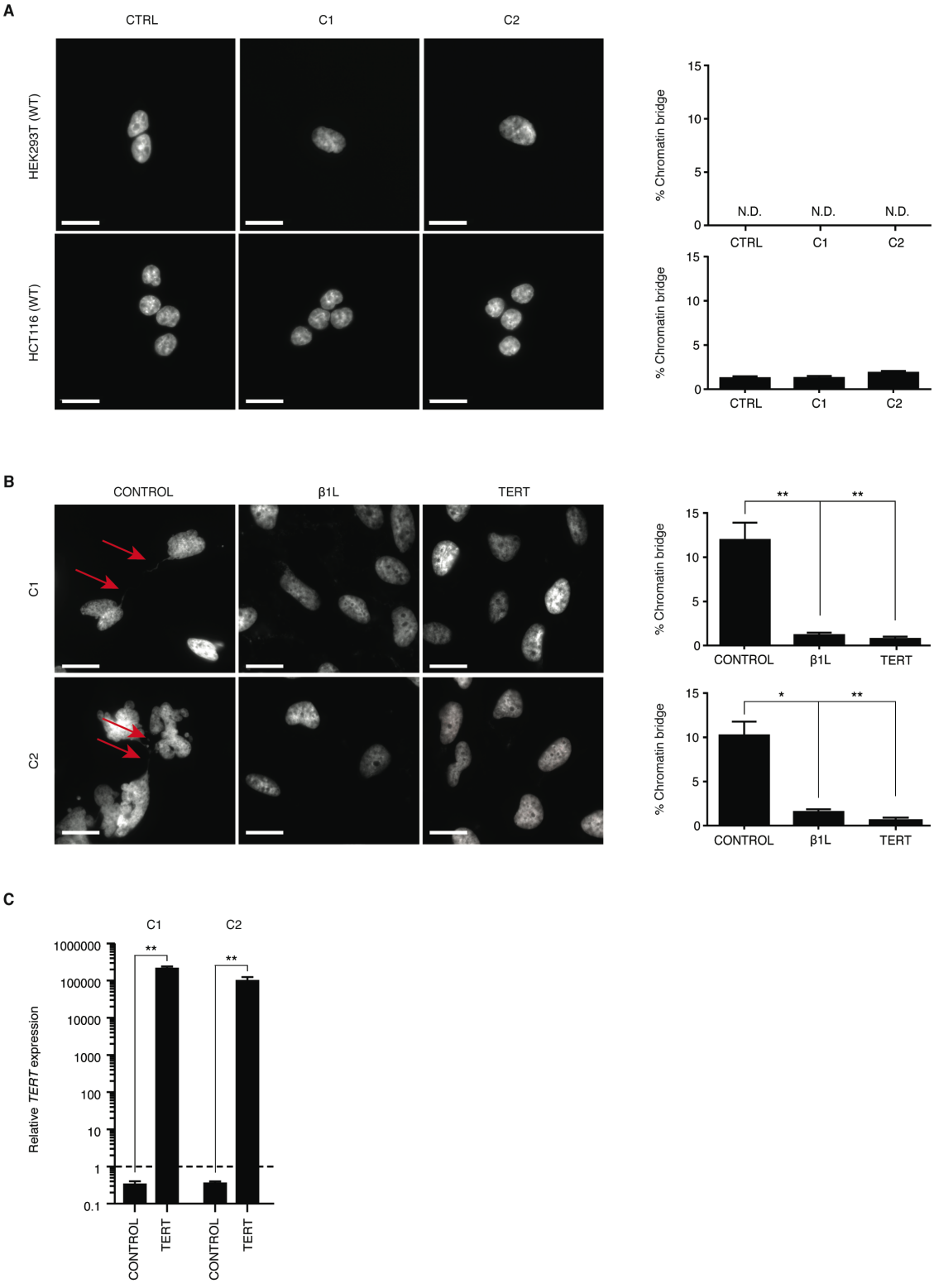

Figure S4, related to Figure 4. Expression of exogenous GABPβ1L or TERT is sufficient to rescue telomere dysfunction in GABPβ1L-reduced LN229 lines.
(A) Representative DAPI images (left images) and quantification (right graphs) of chromatin bridges in CTRL or GABPβ1L-reduced clones derived from HCT116 or HEK293T *TERT* promoter wild-type lines. Scale bar = 20 μm. N.D. = Not detected. Quantification values are weighted mean ± S.D. of at least ten independent fields of view.
(B) Representative DAPI images (left images) and quantification (right graphs) of chromatin bridges in GABPβ1L-reduced LN229 clones transfected with a CONTROL, GABPβ1L, or TERT expression vector. Scale bar = 20 μm. *p value<0.05, **p value<0.01, two-sided Student's t-test relative to CONTROL. Quantification values are weighted mean ± S.D. of at least ten independent fields of view.
(C) *TERT* expression measured by RT-qPCR 7 days post-transfection of GABPβ1L-reduced LN229 clones (58 days post-editing) with either a CONTROL or TERT expression vector. **p value<0.01, two-sided Student's t-test relative to CONTROL. Values are mean ± S.D. of three independent experiments.

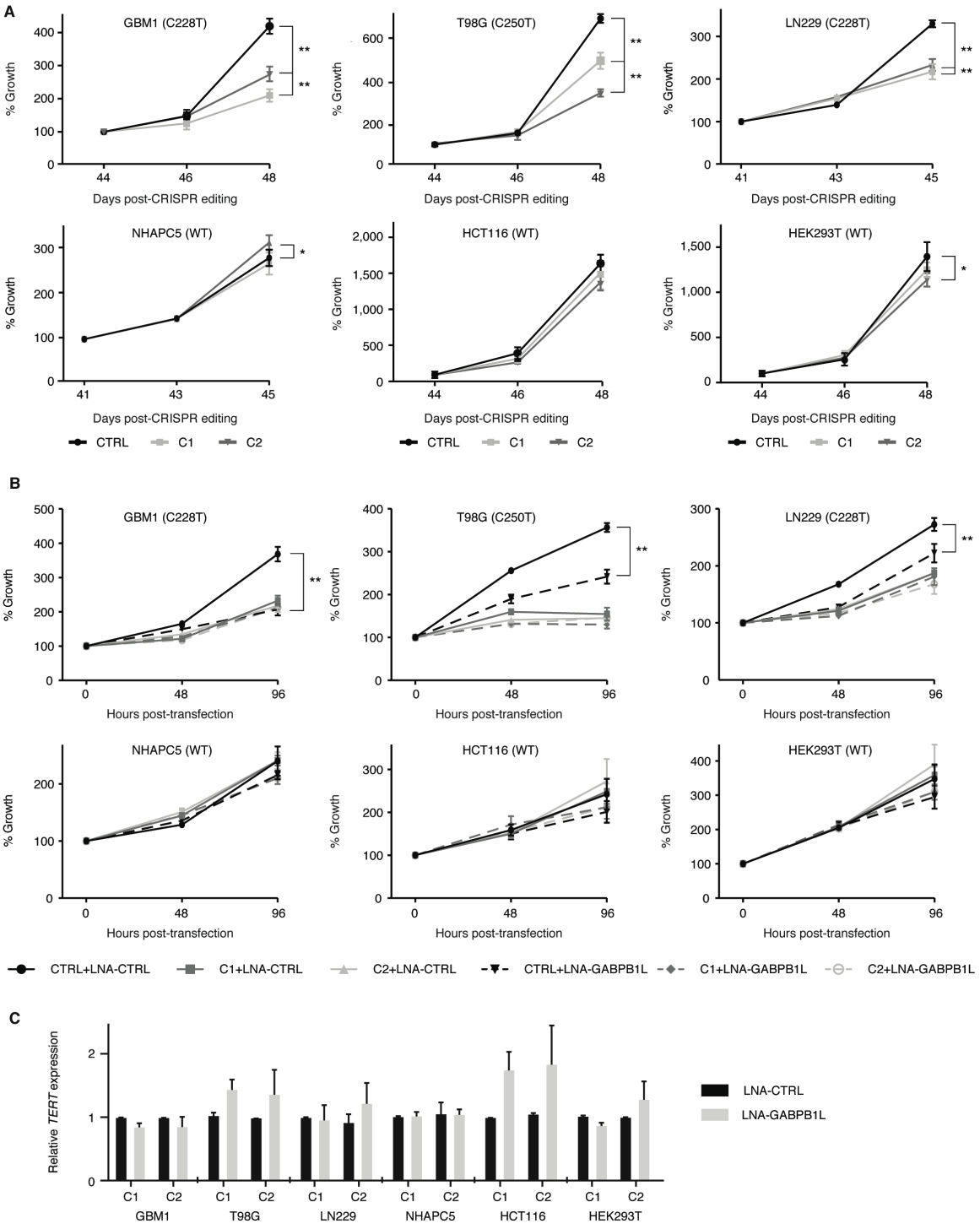

Figure S5, related to Figure 5. GABPβ1L reduction induces growth defects in *TERT* promoter mutant lines.

(A) Percent growth of *TERT* promoter mutant (top graphs) and wild-type (bottom graphs) CRISPR control (CTRL) or GABPβ1L-reduced clones (C1 and C2) relative to the initial time point. *p value<0.05, **p value<0.01, two-sided Student's t-test compared to CTRL (final time point).

(B) Percent growth of *TERT* promoter mutant (top graphs) and wild-type (bottom graphs) CRISPR control (CTRL) or GABPβ1L-reduced clones (C1 and C2) relative to the initial time point following transfection with a scrambled control (LNA-CTRL) or *GABPB1L*-targeting (LNA-GABPB1L) LNA-ASO. Growth was measured 0, 48, and 96 hr post-transfection. *p value<0.05, **p value<0.01, two-sided Student's t-test compared to a control LNA-ASO (LNA-CTRL) at the final time point for each clone (CTRL or GABPβ1L-reduced).
(C) Relative *TERT* expression of GABPβ1L-reduced clones following transfection with a scrambled control (LNA-CTRL) or *GABPB1L*-targeting (LNA-GABPB1L) LNA-ASO.
All values are mean ± S.D. of three independent experiments.

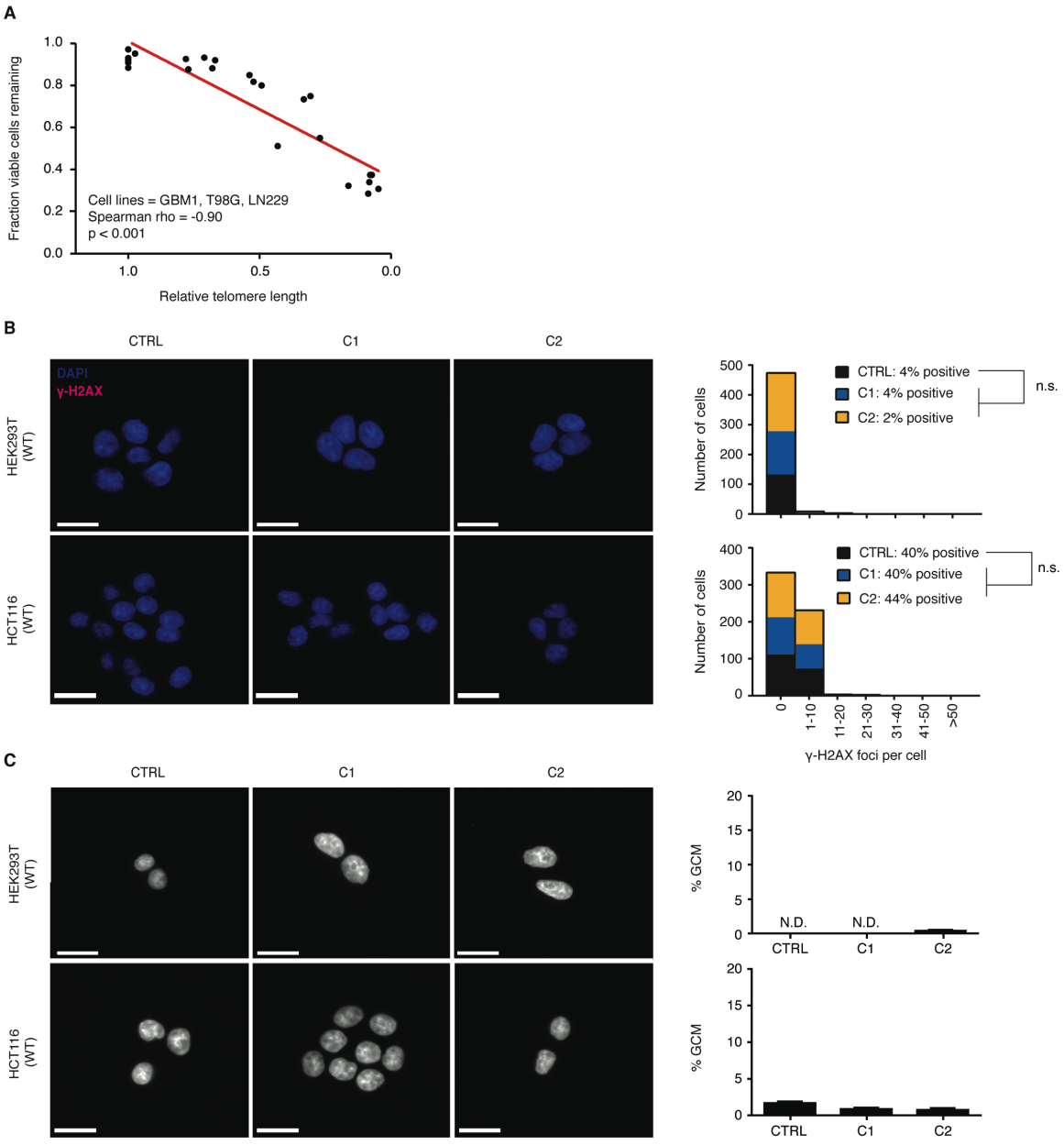

Figure S6, related to Figure 6. GABPβ1L reduction does not induce DNA damage and mitotic cell death in *TERT* promoter wild-type cell lines.

(A) Correlation of relative telomere length and cellular viability across GABPβ1L-reduced clones from all *TERT* promoter-mutant cell lines (GBM1, T98G, and LN229). Spearman rho=-0.90, p value<0.001.

(B) Representative images (left images) and quantification (right graphs) of γ-H2AX staining in CTRL or GABPβ1L-reduced HCT116 and HEK293T clones. Scale bar = 20 μm. n.s. = not significant, two-sided Student's t-test compared to CTRL. Quantification values are sums of at least ten independent fields of view.

(C) Representative DAPI images (left images) and quantification (right graphs) of giant cell micronucleation (GCM) in CTRL or GABPβ1L-reduced HCT116 and HEK293T clones. Scale bar = 20 μm. N.D = Not detected. Quantification values are weighted mean ± S.D. of at least ten independent fields of view.

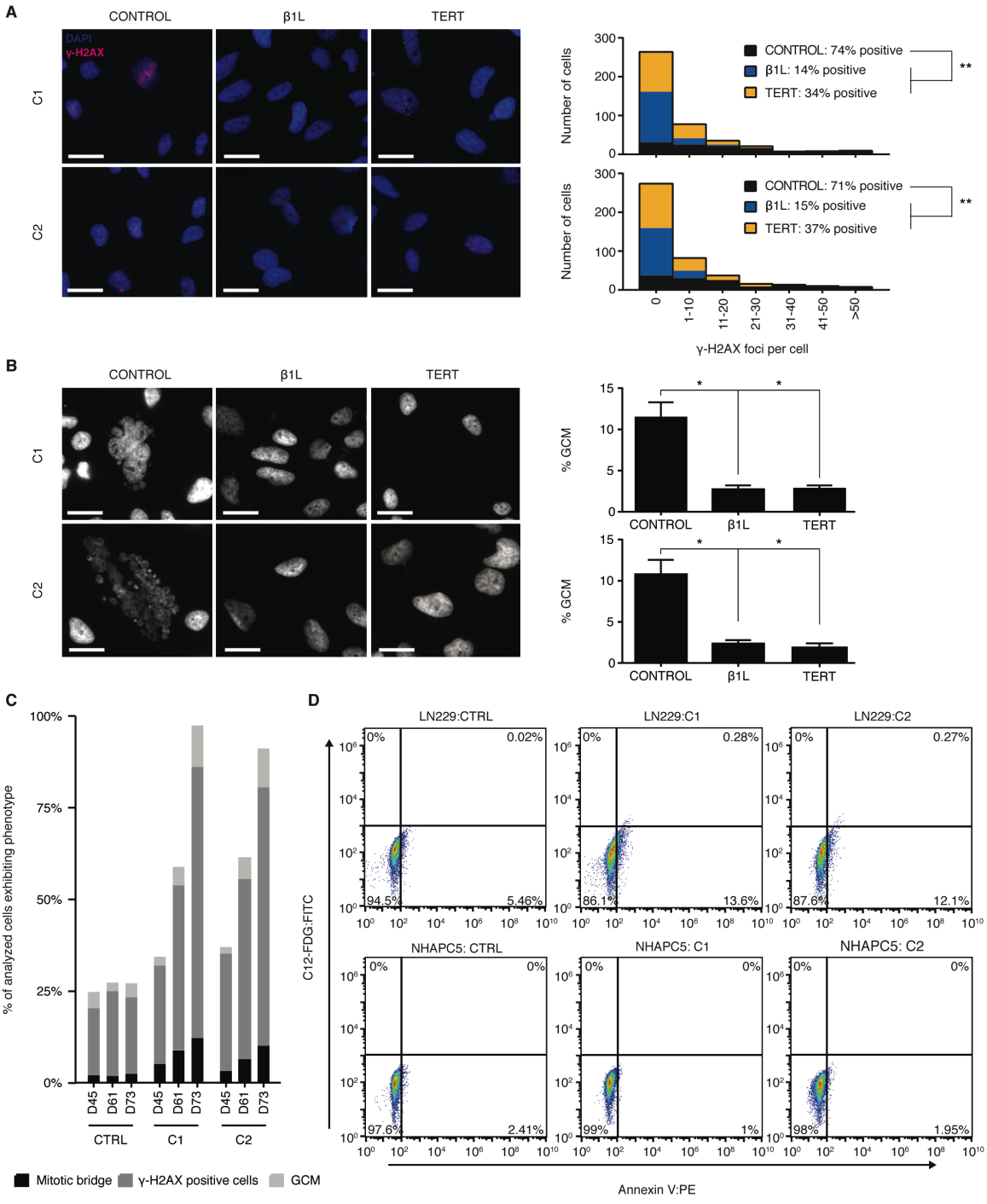

Figure S7, related to Figure 6. Expression of exogenous GABPβ1L or TERT is sufficient to rescue DNA damage and mitotic cell death in GABPβ1L-reduced LN229 clones.

(A) Representative images (left images) and quantification (right graphs) of γ-H2AX staining in GABPβ1L-reduced LN229 clones transfected with a CONTROL, GABPβ1L, or TERT expression vector at 73 days post-editing. Scale bar = 20 μm. *p value<0.05,

**p value<0.01, Student's t-test relative to CONTROL. Quantification values are sums of at least ten independent fields of view.
(B) Representative DAPI images (left images) and quantification (right graphs) of giant cell micronucleation (GCM) in GABPβ1L-reduced LN229 clones transfected with a CONTROL, GABPβ1L, or TERT expression vector at 73 days post-editing. Scale bar = 20 μm. *p value<0.05, Student's t-test relative to CONTROL. Quantification values are weighted mean ± S.D. of at least ten independent fields of view.
(C) Quantification of chromatin bridge formation, γ-H2AX staining (% positive cells), and giant cell micronucleation (GCM) in LN229 CTRL and GABPβ1L-reduced lines at days 45, 61, and 73 post-editing. Values are mean of at least five independent fields of view.
(D) Dot plots quantifying expression of the apoptosis/necrosis marker annexin-V (PE; x-axis) and the senescence marker SA-β-Gal (C-12FDG [FITC]; y-axis) as determined by flow cytometry at day 75 post-editing.

3.8 SUPPLEMENTAL TABLES

Table S6, related to Figure 6. Descriptions for cell lines used for CRISPR-Cas9 editing, including p53 and RB pathway status and alterations.

Cell line	ATCC No.	Description	TERT promoter mutation?
GBM1	N/A	Human patient-derived primary GBM culture	C228T
T98G	CRL-1690	Human primary GBM line	C250T
LN229	CRL-2611	Human primary GBM line	C228T
HCT116	CCL-247	Human colon cancer line	No
HEK293T	CRL-3216	Human embryonic kidney line	No
NHAPC5	N/A	Normal human astrocyte line; stably expressing E6 and E7 viral proteins and mtIDH (R132H variant); selected post-crisis and expressing TERT from the endogenous TERT promoter (Ohba et al. 2016)	No

Cell line	Active RB pathway?	RB pathway alteration	Active p53 pathway?	p53 pathway alteration
GBM1	No	*CDKN2A* homozygous deletion	No	*TP53* p.C141F homozygous mutation
T98G	No	*CDKN2A* homozygous deletion	No	*TP53* p.M237I homozygous mutation
LN229	No	*CDKN2A* homozygous deletion	No	*TP53* p.P98L mutation with LOH
HCT116	No	*CDKN2A* p.R24fs*20 homozygous mutation	Yes	High MDM4 expression (Mancini et al. 2009)
HEK293T	Yes	N/A	Yes	N/A
NHAPC5	No	E7 protein expression	No	E6 protein expression

CHAPTER 4: MATERIALS AND METHODS

4.1 EXPERIMENTAL MODEL AND SUBJECT DETAILS

Cell lines and primary cell cultures

GBM1 (male), T98G (male), LN229 (female), and LN18 (male) cells were cultured in DMEM/Ham's F-12 1:1 media, 10% FBS, 1% Penicillin/Streptomycin. The GBM1 primary culture was previously described in Bell et al. 2015 (Bell et al., 2015). HEK293T (female) and NHAPC5 (male) cells were cultured in DMEM H-21 media, supplemented with 10% FBS, 1% Non- Essential Amino Acids, 1% Glutamine and 1% Penicillin/Streptomycin. The NHAPC5 culture was previously described in Ohba et al. 2016 (Ohba et al., 2016). HCT116 cells (male) were cultured in McCoy's 5A media supplemented with 10% FBS and 1% Penicillin/Streptomycin.

SF7996 (male; passage 6), SF8249 (male; passage 4), SF8279 (male; passage 4), SF9030 (male; passage 3), and SF11411 (female; passage 4) are *TERT* promoter-mutant, *IDH1*-wild-type patient-derived early passage glioma neurosphere (GNS) GBM cultures and were previous described in Fouse et al. 2014 (Fouse et al., 2014). SF7996 (GNS) and GBM1 (serum) are derived from the same piece of tumor tissue from one patient and differ only in derivation conditions. SF10417 (male; passage 9) is a *TERT* promoter-mutant, *IDH1*-mutant patient-derived early passage recurrent high-grade GNS oligodendroglioma culture. hNPCs (male) are human Neural Precursor Cells derived from human induced pluripotent stem cells as previous described (Xu et al., 2016). All GNS cells and hNPCs were cultured in Neurocult NS-A (Stem Cell Technologies) supplemented with 2 mM L-Glutamine, 1% Penicillin/Streptomycin, B-27 without vitamin A (Invitrogen), N2 supplement, 20 ng/mL EGF, and 20 ng/mL bFGF, and 1% sodium

pyruvate. SF10417 was additionally supplemented with 20 ng/mL PDGF-AA. hNPCs were additionally supplemented with 5 ng/mL heparin. Cells were grown on 1.6 ug/cm^2 laminin-coated flasks and dissociated with StemPro Accutase (Gibco). All cells were maintained at 37º Celsius, 5% CO_2. LN229, T98G, HEK293T, LN18 and HCT116 were acquired from ATCC through the UCSF Cell Culture Facility and validated for cell identity via STR testing. The GBM1, SF7996, SF8249, SF8279, SF9030, SF11411, and SF10417 cells are patient-derived cultures validated to be tumor by exome-seq and/or RNA-seq. hNPCs (Xu et al., 2016) were a generous gift from Haoqian Xu and Michael Oldham at University of California, San Francisco. All cells tested negative for mycoplasma contamination.

Animals

Mice and Animal Housing

Athymic (*nu*/*nu*) female mice at 5 weeks of age were purchased from Simonson Laboratories (Figures 7A-C) and Harlan Laboratories (Figures 7D and E). Five mice were grouped per cage. Humane endpoints for sacrifice were established as >15% body weight loss from last weighing and/or the presence of gross neurological symptoms such as hunching, asocial behavior, or spastic behavior. All protocols regarding animal studies were approved by the UCSF Institutional Animal Care and Use Committee (IACUC; protocol AN111064-03B) for Dr. Theodore Nicolaides at the University of California, San Francisco.

Orthotopic xenografting and in vivo imaging

144 hr prior to orthotopic xenografting, LN229 control and GABPβ1L-reduced lines were stably transduced with Firefly Luciferase Lentifect™ Purified Lentiviral Particles catalog # LPP-FLUC-Lv105 (Genecopoiea) with MOI=5. Separately, 240 hr prior to orthotopic xenografting, LN229 control and β1L-reduced lines were stably transduced with either EF1a-TERT-RFP-Bsd catalog # LV1131-RB (GenTarget) or EF1a-empty-RFP-Bsd catalog # LVP-427 lentiviral particles with MOI=0.5. Transduced cells were selected in 5 μg/mL blasticidin (Sigma-Aldrich) for 72 hr, validated for *TERT* and *RFP* expression via RT-qPCR and fluorescent imaging, respectively, and stably transduced with Firefly Luciferase Lentifect™ Purified Lentiviral Particles catalog # LPP-FLUC-Lv105 (Genecopoiea) with MOI=5. All cells were verified for stable luciferase expression prior to injection. 30,000 LN229 CRISPR control or β1L-reduced cells 51 days post-editing per mouse (CTRL=12 mice; C1=12 mice; C2=10 mice) or 50,000 LN229 stably transduced TERT (T) or empty vector (V) CRISPR control or GABPβ1L-reduced cells (7 mice per group) were injected into the frontal cortex. Animal's body weight was measured 3 times per week, tumor size via bioluminescent imaging (BLI) on a Xenogen IVIS Spectrum Imaging System was evaluated 2 times per week, and general behavior and symptomatology was evaluated daily. All BLI images were taken with small binning and a normalized exposure of 30 s recorded 12 min after intraperitoneal injection of 5 μL/g of 30 mg/mL D-Luciferin catalog # LUCK-100 (GoldBio).

4.2 METHOD DETAILS

TCGA expression data set

The collection of the data from The Cancer Genome Atlas (TCGA) (Cancer Genome Atlas Research, 2008) was compliant with all applicable laws, regulations, and policies for the protection of human subjects, and necessary ethical approvals were obtained. Analysis of all data analysis was done in R project version 3.3.2 (http://www.r-project.org/). RSEM normalized RNA-seq expression data for GABP isoforms (GABPA: uc002yly; GABPB1S: uc001zyc, uc001zyd, uc001zye, uc001zyf; GABPB1L: uc001zya, uc001zyb; GABPB2: uc001ewr, uc001ews, uc001ewt) and *TERT* were downloaded along with clinical information from TCGA (level 3 normalized data, December 2015, http://tcga-data.nci.nih.gov/tcga/dataAccessMatrix.htm) for 143 GBM (109 *TERT*-expressing and 34 *TERT*- non-expressing) samples, 49 oligodendroglioma (49 *TERT* promoter-mutant samples), and 249 colorectal cancer (249 *TERT*-expressing) samples. *TERT* mutation status was obtained, when available, from Ceccarelli et al for the glioma samples (Ceccarelli et al., 2016). GABP isoforms were analyzed for monotonic associations with *TERT* using Spearman's correlation. H_0: Spearman's Rho=0; H_1: Spearman Rho≠0; α=0.05. A linear trend-line was generated using the PCA orthogonal regression line.

Transcriptome sequencing and analysis

Total cellular RNA was isolated from GBM1, T98G, and LN229 CRISPR control and GABPβ1L-reduced clones 45 days post-editing via standard TRIzol protocol (ThermoFisher). Prior to library synthesis, RNA was treated with DNase (Roche),

scored on an Agilent 2100 Bioanalyzer for quality control, and quantified on a Qubit® Fluoremeter using the Qubit RNA HS Assay kit (ThermoFisher). Only the samples with RIN >7 were used for RNA-seq. RNA-seq libraries were prepared with the KAPA Stranded mRNA-Seq kit for Illumina platforms (KAPA Biosystems) according to manufacturer's instructions. Briefly, 1 μg RNA was used for mRNA capture. After fragmentation, first strand synthesis, second strand synthesis, and A-tailing, Illumina adaptors with dual indexes were ligated. The libraries were amplified 11 cycles before pooling with 8-10 samples/lane for sequencing. All libraries were sequenced at the UCSF Center for Advanced Technology on an Illumina HiSeq4000 sequencer with paired-end reads and an average read length of 50 base pairs.

Adapter and polyA sequences were removed from reads using cutadapt v1.8.1, with the minimum overlap between adapter and the 3′ of the read set to 1 nt. Reads shorter than 20 nts after adapter trimming were discarded. Reads were aligned with TopHat (v2.0.14) using a GENCODE V19 transcriptome-guided alignment with parameters –r 200 –library-type fr-firststrand, --prefilter-multihits genome. To estimate transcript abundance, aligned data was processed with FeatureCounts (v1.4.6) with parameters -s 2 -B -p -O -T 24 using a GENCODE V19 GTF reference.

EdgeR was used to determine differential expression between the six GABPβ1L-reduced clones and three CRISPR control clones from *TERT* promoter mutant lines. All three CRISPR control clones were used as a reference ("REF") in comparison to the six β1L-reduced clones ("TEST"). Genes with <1cpm/3 samples were discarded from the analysis prior to library size calculation. The Beyer-Hardwick Method was used to determine genes significantly altered between the "REF" and "TEST" with FDR<0.05.

Non-directional GO-TermFinder was used to determine GO-enriched processes for differentially expressed genes. GABPA-bound genes were determined from ENCODE GABPA ChIP-seq data for all available cancer cell lines (http://hgdownload.cse.ucsc.edu/goldenPath/hg19/encodeDCC/wgEncodeRegTfbsClustered/wgEncodeRegTfbsClusteredV3.bed.gz). BEDOPS closest-features was used to determine transcription start sites within 3 kb of called GABPA peaks presented in ≥2 samples. These transcription start sites are referred to “GABP-bound genes” throughout the text.

siRNA and LNA-ASO knockdown

Non-targeting, *GABPB1*, and *GABPB2*-directed siRNA pools were obtained from Dharmacon. Scrambled control and *GABPB1L* 3’ UTR-directed Locked Nucleic Acid Antisense Oligonucleotides (LNA-ASOs) were obtained from Exiqon. 100 µL of cells were seeded at a density of 30,000 cells/mL in a 96-well plate and transfected 24 hr after with a final concentration of 50 nM siRNA or 25 nM LNA-ASO and 0.1 uL of Dharmafect 1 reagent (Dharmacon). At 48 and 72 hr post-transfection, cells were lysed and cDNA was generated using the POWER SYBR Green Cells-to-Ct kit (Ambion). Quantitative PCR was performed to measure the expression levels of *GUSB*, *TERT*, *GABPB1L*, and *GABPB2* as described below. All siRNAs and LNA-ASOs were independently validated at 48 and 72 hr post-transfection for >50% knockdown of target transcript in all cell lines.

RT-qPCR

Quantitative PCR was performed with POWER SYBR Green Complete Master Mix (LifeTechnologies) to measure the expression levels of *GUSB* (forward primer: CTCATTTGGAATTTTGCCGATT; reverse primer: CCGAGTGAAGATCCCCTTTTTA), *TERT* (forward primer: TCACGGAGACCACGTTTCAAA; reverse primer: TTCAAGTGCTGTCTGATTCCAAT), *GABPB1* (forward primer: TCCACTTCATCTAGCAGCACA; reverse primer: GTAATGGTGTTCGGTCCACTT), *GABPB1L* (forward primer: ATTGAAAACCGGGTGGAATC; reverse primer: CTGTAGGCCTCTGCTTCCTG), *GABPB2* (forward primer: CGCCACCATCGAGATGTCG; reverse primer: TCCAGAGCTATGTCAAAGGCT), *SKP2* (forward primer: ATGCCCCAATCTTGTCCATCT; reverse primer: CACCGACTGAGTGATAGGTGT), *COXIV* (forward primer: CAGGGTATTTAGCCTAGTTGGC; reverse primer: GCCGATCCATATAAGCTGGGA), *EIF6* (forward primer: CCGACCAGGTGCTAGTAGGAA; reverse primer: CAGAAGGCACACCAGTCATTC), *TFB1M* (forward primer: GTTGCCCACGATTCGAGAAAT; reverse primer: GCCCACTTCGTAAACATAAGCAT), and *RPS16* (forward primer: TCGGACGCAAGAAGACAGC; reverse primer: AGCAGCTTGTACTGTAGCGTG). Each sample was measured in triplicate on the Applied Biosystems 7900HT Fast Real-Time System. Melting curves were manually inspected to confirm PCR specificity. Relative expression levels were calculated by the deltaCT method against *GUSB*.

CRISPR-Cas9 editing

Plasmids encoding spCas9 and sgRNAs were obtained from Addgene (Plasmids #41815 and #47108). Oligonucleotides for construction of sgRNAs were cloned into the sgRNA plasmid as previously described (Brown et al., 2016). Target sequences for sgRNAs are provided in Table S1. Targeting vectors PuroR TV and HygroR TV were acquired and incorporated at target loci as previously described (Gapinske et al., 2018). In brief, LN229, NHAPC5, HEK293T, HCT116, and T98G cells were transfected with Lipofectamine 2000 (Invitrogen) according to the manufacturer's instructions in 24 well plates. GBM1 cells were transfected by electroporation using a Gene Pulser XCell (BioRad) in PBS at 140 Volts, 950 μF. Each cell line was transfected with equal amounts of Cas9, target sgRNA, targeting vector PuroR TV (GBM1, LN229, HCT116, HEK293T, and T98G) or HygroR TV (NHAPC5) and universal sgRNA. Cleaving of the targeting vector by the universal sgRNA-directed Cas9 allowed for integration of the PuroR or HygroR cassette at the control or *GABPB1L* target loci. Integration only occurs post-cutting of both the targeting vector and target genomic locus. Clonal populations were selected with Puromycin (0.5 μg/ml HCT116 and T98G, 1 μg/ml GBM1 and LN229, and 2 μg/ml HEK293T) or Hygromycin (0.5 μg/ml for NHAPC5).

Analysis of on-target and off-target editing

Analysis of on-target and off-target mutations was conducted as previously described (Gapinske et al., 2018). In brief, genomic DNA from each clone was isolated using the Animal Genomic DNA Purification Mini Kit (Earthox Life Sciences). PCRs to detect integration of the targeting vector at on-target or off-target sites were performed using

KAPA2G Robust PCR kits (Kapa Biosystems) according to the manufacturer's instructions. The DNA sequences of the primers for each target are provided in Table S1. PCR products were visualized in 2% agarose gels and images were captured using a ChemiDoc-It2 (UVP). Indels at off-target sites were analyzed with the Surveyor Mutation Detection kit (IDT) by first amplifying the target locus using PCR with KAPA Robust2G DNA polymerase. The resulting PCR products were melted and re-annealed according to manufacturer's instructions, and 18 μL of the reannealed duplex was mixed with 1μL of Surveyor Nuclease and 1 μL of Enhancer Solution and incubated at 42° Celsius for 1 hr. Final product was loaded onto a 10% TBE polyacrylamide gel and run at 200 V for 30 min. The gels were stained with ethidium bromide and visualized using a ChemiDoc-It2 (UVP). On-target editing of *GABPB1L* (Figure S2A) or control locus (Figure S3B) was evaluated by PCR to detect the integration of the targeting vector. DNA sequencing of the alleles without integration was used to detect indels (Figure S2B). Analysis of off-target mutations was performed by testing integration of the targeting vector at predicted off-target sites (Hsu et al., 2013) in coding regions for each sgRNA used in each cell line (Figures S3A and S3D-F). For predicted off-target sites within coding sequences we performed Surveyor assays to detect indels (Figure S3C).

Immunoblotting

Immunoblotting for Cyclophilin B (loading control) and GABPβ1 (GABPβ1S and GABPβ1L) was performed using a rabbit anti-Cyclophilin B antibody PA1-027A (Pierce antibodies; 1:1,000 dilution) and rabbit anti-GABPβ1 antibody 12597-1-AP (Proteintech; 1:500 dilution) using the NuPAGE system (Thermofisher), according to the provider's

instructions. Detection of primary bands was done using the Li-Cor goat anti-rabbit 680RD secondary antibody (1:15,000 dilution) on the Li-Cor Odyssey Fc imaging system.

NanoBiT protein-protein interaction assay

Full-length *GABPB1L* or *GABPB1S* was cloned into either the pBiT1.1-C [TK/LgBiT] or pBiT2.1-C [TK/LgBiT] vectors (Promega; N196A and N197A, respectively) using In-Fusion HD Cloning (Takara). In accordance with the manufacturer's instructions, the QuikChange Lightning Site-Directed Mutagenesis kit (Agilent) was used to introduce three separate deletions (DEL1-3) into the pBiT1.1-C-GABPB1L vector (see Table S3 for mutagenesis primers). Mutagenized plasmids were validated using Sanger sequencing and purified for use in the NanoBiT assay. Prior to use, 1 volume NanoBiT vector was diluted into 3 volumes of pCMV6-Neo control vector (OriGene) to a final volume of 10 ng/μL. 100 μL of LN229 or NHAPC5 cells were seeded at a density of 30,000 cells/mL in 96-well plates 24 hr prior to transfection. Cells were transfected with a total of 100 ng of plasmid DNA and 0.3 μL X-tremeGENE HP DNA Transfection Reagent (Roche) according to manufacturer's instructions. The following combinations were used to assay GABPβ1L tetramer formation in LN229 and NHAPC5 cells:

POS: pBiT1.1-C-GABPB1L-WT + pBiT-2.1-C-GABPB1L

NEG: pBiT1.1-C-GABPB1L-WT + pBiT-2.1-C-GABPB1S

DEL1: pBiT1.1-C-GABPB1L-DEL1 + pBiT-2.1-C-GABPB1L

DEL2: pBiT1.1-C-GABPB1L-DEL2 + pBiT-2.1-C-GABPB1L

DEL3: pBiT1.1-C-GABPB1L-DEL3 + pBiT-2.1-C-GABPB1L

24 hr following transfection, Nano-Glo® Live Cell Substrate diluted in Nano-Glo® LCS Dilution Buffer (Promega; N205A and N206A, respectively) was added directly to the cells and luminescence was assayed 1 hr later on a GloMax® 96 MicroPlate Luminometer (Promega) according to manufacturer's instructions. All data were normalized to the positive control (POS) for each cell line.

Cell proliferation and viability assays

100 µL of cells were seeded at a density of 5,000 cells/mL in 96-well plates. At t=0, 48 and 96 hr post-seeding, MTS (Cell titer 96 aqueous MTS, Promega) was incubated for 2 hr at 37º Celsius in a ratio of 1:5 in media, according to manufacturer's instructions. Plate was read on the Bioplate Synergy 2 microplate reader at 490 nm. Cell proliferation of individual samples was calculated by normalizing absorbance to their corresponding absorbance at t=24 hr. Each time point was analyzed in triplicates. For cell viability, cells were trypsinized, collected and counted on a hemocytometer with trypan-blue exclusion approximately every 7 days from day 33 to day 102 post-editing, or until the minimal sensitivity limits of the assay were reached. Between viability time points, cells were split prior to confluency and replated at $1/8^{th}$ density to ensure consistent growth conditions. The ratio between viable and dead cells was used to determine cell viability. It is important to note that trypsinization of cells undergoing telomere dysfunction may have influenced to the viability phenotype in the GBM1 and T98G clones after day 85 post- editing.

Chromatin immunoprecipitation

Chromatin immunoprecipitation (ChIP) for GABPα was performed using the ActiveMotif High Sensitivity kit. In brief, GBM1, T98G, HCT116, and HEK293T CRISPR controls and GABPβ1L-reduced clones were grown to 80% confluency in 15 cm plates and fixed with 4% formaldehyde. Chromatin was sonicated to a size range of 200-1200 bp by the Diagenode Biorupter. 12-18 µg of chromatin was used per GABPα (Santa Cruz Biotechnology: sc-22810) and IgG control (Cell Signaling: 2729) immunoprecipitation for each cell type. Enrichment at the *TERT* promoter was determined by qPCR with the ssoAdvanced Universal SYBR Green Supermix (Biorad) supplemented with Resolution Solution from GC-RICH PCR System (Roche). The following primer set was used for qPCR: *TERT+47* (forward: 5'-GCCGGGGCCAGGGCTTCCCA-3'; reverse: 5' CCGCGCTTCCCACGTGGCGG-3'; Tm=74° Celsius). PCR was carried out on the Applied Biosystems 7900HT Fast Real-Time System. Three replicate PCR reactions were carried out for each sample.

Telomere length measurement

All telomere length measurements were conducts using the telomere qPCR protocol initially described in Cawthon 2002 (Cawthon, 2002) and later modified in Lin et al. 2009 (Lin et al., 2010). DNA was collected from CRISPR control and β1L-reduced cell lines at days 33, 44, 61, 78, and 83 post-CRISPR-Cas9 editing using Phenol:Chloroform:Isoamyl Alcohol (Invitrogen) according to manufacturer's instructions. DNA was diluted to a final concentration of 2 ng/µL prior to analysis. Telomere length was measured by qPCR with POWER SYBR Green master mix on the

Applied Biosystems 7900HT Fast Real-Time System using the following telomere (TEL) and single gene control (SGC) primer sets: TEL-qPCR, primer forward: CGGTTTGTTTGGGTTTGGGTTTGGGTTTGGGTTTGGGTT, primer reverse: GGCTTGCCTTACCCTTACCCTTACCCTTACCCTTACCCT; SGC-qPCR, primer forward: CAGCAAGTGGGAAGGTGTAATCC primer reverse: CCCATTCTATCATCAACGGGGTACAA (Cawthon, 2002; Lin et al., 2010; Xie et al., 2015). The following PCR conditions were used: 95° Celsius for 10 min followed by 40 cycles of data collection at 95° Celsius for 15 s, 60° Celsius anneal for 30 s and 72° Celsius extend for 30 s along with 80 cycles of melting curve from 60° Celsius to 95° Celsius. Relative telomere length was determined as the linear relationship between TEL and SGC (T/S). Three independent RT-qPCR reactions were carried out for each sample, with each independent experiment performed on distinct days with distinct populations of cells.

Exogenous GABPβ1L and TERT overexpression

GABPB1L human cDNA (OriGene) was cloned into pCMV6-Neo Vector (OriGene) using the Cold Fusion Cloning Kit (System Biosciences) according to manufacturer's instructions. The pCMV6-Neo-GABPB1L plasmids obtained were validated by Sanger sequencing using the manufacturer's primers. 2 µg pCMV6-Neo (empty vector, for control purposes), pCMV6-Neo-B1L or pCI-Neo-hEST2 (Addgene) were transfected into each GBM1, T98G, and LN229 CRISPR control clone (CTRL) or GABPβ1L-reduced clone (C1 and C2) using 6 µL X-tremeGENE HP DNA Transfection Reagent (Roche) according to producer's instructions at day 61 (GBM1 and T98G) or day 58 (LN229)

post-editing. C1/C2 and β1L/TERT refers to the clone number and cDNA transfected, respectively. Overexpression of exogenous GABPβ1L and TERT mRNA was confirmed by RT-qPCR as described above. Clones were maintained in 100 μg/mL G418 (Invivogen) and validated for continued *GABPB1L* and *TERT* expression three weeks post-transfection. Lentiviral TERT rescue is described above under the "Orthotopic xenografting and *in vivo* bioluminescent imaging" subheading. pCI neo-hEST2 was a gift from Robert Weinberg (Meyerson et al., 1997) (Addgene plasmid # 1781).

Fluorescent imaging and quantification

CTRL and GABPβ1L-reduced clones were seeded at a density of 25,000 cells/mL on day 70 post-editing. Cells were fixed in 4% formaldehyde and permeabilized in 100% methanol before co-staining with DAPI and anti-γH2AX AF647 conjugated antibody (EMD Millipore 05-636-AF647) at 4° Celsius overnight. All images were taken at 63x magnification on an AxioImager M1 upright fluorescent microscope (Zeiss) with 2.8 ms exposure. Post-processing and signal normalization of images was done using the on-board ZEN2 software. Quantification of extent of chromatin bridge formation and giant cell micronucleation was performed as follows: each slide was assigned a randomized number to blind the quantifier prior to counting. Ten computationally randomized unique 40x fields of view with a cell number of n>20 were used per slide. For each field of view, total cell number, number of chromatin bridges, and number of giant micronucleated cells were counted. Only nuclei completely in the field of view were counted. A chromatin bridge was defined as a solid strand of nuclear material linking two distinctly independent nuclei. Two nuclei linked by a chromatin bridge were counted as one cell.

A giant micronucleated cell was defined as a single cell containing n≥5 uncondensed nuclei. The weighted proportion of chromatin bridges and giant micronucleated cells was determined per field of view and summed into an aggregate proportion. All methods and quantifications were verified using the same parameters as described above by an independent party. Quantification of γH2AX was performed similarly to chromatin bridge and giant cell micronucleation counting with the following differences: n>10 cells per field of view was used as a threshold and individual visible γH2AX foci were counted per cell per field of view. This procedure was likewise followed to quantify LN229 clones at day 45 and day 61 post-editing (n=4 fields of view).

Flow cytometry

On day 75 post-editing, 300,000 cells/line were stained with a combination of Hoechst® 33342 (Thermofisher; 10 ng/mL), AnnexinV-PE (BD Biosciences #51-65875X; 1:1,000 dilution), and C-12-FDG (Setareh Biotech; 33 μM final concentration) for 45 min at 37° Celsius in the dark. Samples were run for 10,000 counts on a Sony SH800 cytometer and analyzed on FlowJo®. The same gating strategy was used for all experiments. All data were collected ONLY after a stable flow of cells had been established. Then, FSC-A vs. FSC-H gating was used to select for singlets along the positive diagonal. Next, FSC-A vs. SSC-A gating was used to remove all cellular debris (FSC-A/SSC-A low particles). Finally, non-specific antibody/fluorophore uptake was used to gate against dead cells with compromised membranes.

4.3 QUANTIFICATION AND STATISTICAL ANALYSIS

All statistical analysis was done using GraphPad Prism 7. Non-parametric Spearman correlation was used for GABP isoforms versus *TERT* and telomere length versus viability analysis (α=0.05). Adjusted p values after multiple comparison correction are reported for each correlation. A non-parametric Spearman correlation was chosen due to the failure of a subset of data sets to meet the homoscedasticity assumption of the Pearson test. Mouse survival data for the orthotopic xenograft experiments were analyzed with the Kaplan-Meier Log-Rank Test (α=0.05). The non-parametric Welch's t-test was used as listed for samples with unequal sample sizes (α=0.05). A two-sided heteroscedastic Student's t-test was used as listed for all other assays (α=0.05) after confirming differences in variances between tested groups. All error bars shown are mean ± S.D. A sample size of 3 independent experiments (biological replicates) was used for all experiments, unless otherwise noted, in order to ensure appropriate statistical power to detect a statistically significant change of at least two-fold. 3 technical replicates per biological replicate were used for each experiment as noted.

4.4 DATA AND SOFTWARE AVAILABILITY

All data used for GABP isoform and *TERT* expression correlations are available for public access from the TCGA (level 3 normalized data, December 2015, http://tcga-data.nci.nih. gov/tcga/dataAccessMatrix.htm). All raw data used for RNA-seq analysis has been deposited in the European Genome Archive (EGA) under ID code EGAS0000100258.2. Scripts used for RNA-seq analysis are available at https://github.com/UCSF-Costello-Lab/Tert-gabp.

4.5 KEY RESOURCES TABLE

REAGENT or RESOURCE	SOURCE	IDENTIFIER
Antibodies		
Cyclophilin B	Pierce antibodies	PA1-027A
GABPB1	Proteintech	12597-1-AP
Goat anti-rabbit secondary antibody	Li-Cor	680RD
GABPα	Santa Cruz Biotechnology	sc-22810
IgG	Cell Signaling	2729
REAGENT or RESOURCE	**SOURCE**	**IDENTIFIER**
γH2AX AF647	EMD Millipore	05-636-AF647
Bacterial and Virus Strains		
Firefly Luciferase Lentifect™ Purified Lentiviral Particles	Genecopoiea	LPP-FLUC-Lv105
Biological Samples		
Chemicals, Peptides, and Recombinant Proteins		
Dharmafect 1	Dharmacon	T-2001-02
POWER SYBR Green Complete Master Mix	Applied Biosystems	4367659
Lipofectamine 2000	Invitrogen	11668-030
Puromycin	Millipore-Sigma	P8833
Hygromycin B Solution	Omega Scientific	HG-80
KAPA Robust2G DNA polymerase	KAPA	KK5023
In-Fusion HD Cloning Plus	Takara	638910
X-tremeGENE HP DNA Transfection Reagent	Roche	06366546001
Nano-Glo® Live Cell Substrate	Promega	N205A
Nano-Glo® LCS Dilution Buffer	Promega	N206A
Cell titer 96 aqueous MTS	Promega	G3581
Formaldehyde	Sigma	F8775
ssoAdvanced Universal SYBR Green Supermix	Biorad	1725270
Resolution Solution from GC-RICH PCR System	Roche	19024024
Phenol:Chloroform:Isoamyl Alcohol	Invitrogen	15593-031
TRIzol	LifeTechnologies	15596018
Methanol	Sigma	179337
VECTASHIELD Antifade Mounting Medium with DAPI	Vector Laboratories	H-1200
Hoechst® 33342	Thermofisher	62249
AnnexinV-PE	BD Biosciences	556421
C-12-FDG	Setareh Biotech	7188
D-Luciferin	GoldBio	LUCK-100

REAGENT or RESOURCE	SOURCE	IDENTIFIER
Critical Commercial Assays		
KAPA Stranded mRNA-Seq kit	KAPA Biosystems	KK8421
Power SYBR Green Cells-to Ct kit	Ambion	4402953
In-Fusion HD Cloning	Takara	121416
QuikChange Lightning Site-Directed Mutagenesis	Agilent	210518
ChIP-IT High Sensitivity®	ActiveMotif	53040
Cold Fusion Cloning Kit	System Biosciences	MC010B-1
Surveyor Mutation Detection	IDT	706025
Deposited Data		
RNA-seq data	European Genome Archive (EGA)	EGAS00001002 58.2
Scripts		https://github.com/UCSF-Costello-Lab/Tert-gabp
Experimental Models: Cell Lines		
GBM1	Bell et al., 2015	N/A
T98G	ATCC	ATCC CRL-1690
LN229	ATCC	ATCC CRL-2611
HEK293T	ATCC	ATCC CRL-3216
NHAPC5	Ohba et al., 2016	N/A
HCT116	ATCC	ATCC CRL-247
SF10417-GNS	Costello Lab	N/A
SF7996-GNS	Costello Lab	N/A
SF8249	Costello Lab	N/A
SF9030	Costello Lab	N/A
SF11411	Costello Lab	N/A
LN18	ATCC	CRL-2610
hNPCs	Xu et al., 2016	N/A
Experimental Models: Organisms/Strains		
Mice / athymic (*nu*/*nu*)	Simonsen Laboratories	Sim:(NCr) nu/nu fisol
Mice / athymic (*nu*/*nu*)	Envigo (formerly Harlan)	Hsd:Athymic Nude *Foxn1*^{nu}
Oligonucleotides		
Genomic editing: See Table S1		
GUSB forward: CTCATTTGGAATTTTGCCGATT	Bell et al., 2015	N/A

REAGENT or RESOURCE	SOURCE	IDENTIFIER
GUSB reverse: TTCAAGTGCTGTCTGATTCCAAT	Bell et al., 2015	N/A
TERT forward: TCACGGAGACCACGTTTCAAA	This paper	N/A
TERT reverse: TTCAAGTGCTGTCTGATTCCAAT	This paper	N/A
GABPB1 forward: TCCACTTCATCTAGCAGCACA	This paper	N/A
GABPB1 reverse: GTAATGGTGTTCGGTCCACTT	This paper	N/A
GABPB1L forward: ATTGAAAACCGGGTGGAATC	This paper	N/A
GABPB1L reverse: CTGTAGGCCTCTGCTTCCTG	This paper	N/A
GABPB2 forward: CGCCACCATCGAGATGTCG	This paper	N/A
GABPB2 reverse: TCCAGAGCTATGTCAAAGGCT	This paper	N/A
SKP2 forward: ATGCCCCAATCTTGTCCATCT	This paper	N/A
SKP2 reverse: CACCGACTGAGTGATAGGTGT	This paper	N/A
COXIV forward: CAGGGTATTTAGCCTAGTTGGC	This paper	N/A
COXIV reverse: GCCGATCCATATAAGCTGGGA	This paper	N/A
EIF6 forward: CCGACCAGGTGCTAGTAGGAA	This paper	N/A
EIF6 reverse: CAGAAGGCACACCAGTCATTC	This paper	N/A
TFB1M forward: GTTGCCCACGATTCGAGAAAT	This paper	N/A
TFB1M reverse: GCCCACTTCGTAAACATAAGCAT	This paper	N/A
RPS16 forward: TCGGACGCAAGAAGACAGC	This paper	N/A
RPS16 reverse: AGCAGCTTGTACTGTAGCGTG	This paper	N/A
TERT+47 forward: GCCGGGGCCAGGGCTTCCCA	Bell et al. 2015	N/A
TERT+47 reverse: CCGCGCTTCCCACGTGGCGG	Bell et al. 2015	N/A

REAGENT or RESOURCE	SOURCE	IDENTIFIER
TEL forward: CGGTTTGTTTGGGTTTGGGTTTGGGTTTGGGTTTGGGTT	Cawthon, 2002; Lin et al., 2010; Xie et al., 2015	N/A
TEL reverse: GGCTTGCCTTACCCTTACCCTTACCCTTACCCTTACCCT	Cawthon, 2002; Lin et al., 2010; Xie et al., 2015	N/A
SGC forward: CAGCAAGTGGGAAGGTGTAATCC	Cawthon, 2002; Lin et al., 2010; Xie et al., 2015	N/A
DEL1 forward: GCCTCTGCTTCCTGTTTCTTTAGGAGCTGCTGT	This paper	N/A
DEL1 reverse: ACAGCAGCTCCTAAAGAAACAGGAAGCAGAGGC	This paper	N/A
DEL2 forward: GCAGAGGCCTACAGACAGTTGGAAGCTATGAC	This paper	N/A
DEL2 reverse: GTCATAGCTTCCAACTGTCTGTAGGCCTCTGC	This paper	N/A
DEL3 forward: GTCATAGCTTCCAACTGTAGGCCTCTGCTTCC	This paper	N/A
DEL3 reverse: GGAAGCAGAGGCCTACAGTTGGAAGCTATGAC	This paper	N/A
Recombinant DNA		
siRNA Non-targeting	Dharmacon	D-001206-13
siGABPB1	Dharmacon	L-013083-00
siGABPB2	Dharmacon	M-016074-00
LNA Scramble control: TTTAAGCCGATGCGTT	Exiqon	300603-00
LNA GABPB1L 3' UTR: CTAACCAACAACGATC	Exiqon	300603-00
spCas9	Addgene	#41815
sgRNAs	Addgene	#47108
pBiT1.1-C [TK/LgBiT]	Promega	N196A
pBiT2.1-C [TK/LgBiT]	Promega	N197A
pBiT1.1-C-GABPB1L-WT/DEL1/DEL2/DEL3	This paper	N/A
pBiT-2.1-C-GABPB1L	This paper	N/A
pBiT-2.1-C-GABPB1S	This paper	N/A
pCMV6-Neo control vector	OriGene	PCMV6NEO

REAGENT or RESOURCE	SOURCE	IDENTIFIER
pCMV6-Neo-GABPB1L	This paper	N/A
Software and Algorithms		
R v1.7.1	R Project	https://cran.r-project.org/mirrors.html
TopHat v.2.0.14	https://doi.org/10.1186/gb-2013-14-4-r36	https://ccb.jhu.edu/software/tophat/index.shtml
GENCODE V19	GENCODE	https://www.gencodegenes.org/releases/19.html
edgeR v3.7	https://doi.org/10.18129/B9.bioc.edgeR	https://bioconductor.org/packages/release/bioc/html/edgeR.html
GO-TermFinder v0.86	https://doi.org/10.1093/bioinformatics/bth456	https://metacpan.org/release/GO-TermFinder
BEDOPS v.2.4.32	https://doi.org/10.1093/bioinformatics/bts277	https://bedops.readthedocs.io/en/latest/
FlowJo v10	FlowJo, LLC	https://www.flowjo.com/solutions/flowjo/downloads
Prism v7	GraphPad	https://www.graphpad.com/how-to-buy/

CHAPTER 5: DISCUSSION

5.1 CONTRIBUTION TO FIELD OF TUMOR IMMORTALITY

Telomerase reactivation occurs in more than 90% of human cancers and is fundamental for tumor cell immortalization. While the occurrence of *TERT* promoter mutations early in GBM evolution suggests they are important for tumorigenesis, their role in maintaining telomere length, replicative immortality, and cell viability at later time points has been relatively unexplored. We have identified the tetramer-forming GABPβ1L isoform of GABP to be a necessary component for full activation of the mutant *TERT* promoter and replicative immortality in *TERT* promoter mutant, but not wild-type, GBM cells. These results add to recent studies showing that *TERT* promoter mutations are necessary but not sufficient for cellular immortalization in *TERT* promoter mutant tumor cells (Chiba et al., 2017; Li et al., 2015). Our results also suggest binding of the GABPβ1L-containing GABP tetramer to the mutant *TERT* promoter is necessary to maintain maximal expression of *TERT*.

5.2 CAVEATS, CONSIDERATIONS, AND FUTURE DIRECTIONS

Telomere shortening and loss of cellular proliferation has been previously observed in brain tumor cultures after sustained inhibition of telomerase (Barszczyk et al., 2014; Castelo-Branco et al., 2011; Marian et al., 2010). One difference with these studies and ours is that in addition to potently reducing the expression of *TERT*, our GABPβ1L-reduced clones had concomitant deregulation of a subset of GABP-regulated genes that may influence the observed TERT-dependent phenotypes. Although overexpression of exogenous TERT rescued cell growth of the cells with reduced GABPβ1L function, expression of TERT at more physiologic levels through activation of

the endogenous wild-type *TERT* allele may allow for more precise analysis of phenotypes. Thus, we cannot fully rule out that other GABPβ1L target genes may contribute to the *in vitro* and *in vivo* phenotypes we observed.

The growth decrease occurring as early as 48 hr after LNA-ASO-mediated knockdown of GABPβ1L raises the possibility that, in addition to the gradual and protracted loss of viability, GABPβ1L and TERT reduction also could have immediate effects. As telomere length is heterogeneous within tumor cell cultures (der-Sarkissian et al., 2004; Wang et al., 2013), cells with shorter telomeres may be more vulnerable upon reduction in TERT expression. Conversely, we expect that the subset of GBM cells with longer telomeres – and not those with critically short telomeres – would preferentially survive through the cell expansion required to establish the clonal cultures of GABPβ1L-reduced cells, and then succumb to gradual decreases in telomere length at later time points.

Overall this ongoing process could contribute to the gradual loss of viability detected in the bulk population assays. The more immediate effect in our LNA-ASO cell experiments is consistent with an acute telomere-mediated cell death phenotype in NRAS-mutant melanoma due to dependence on *TERT* expression from the mutant promoter (Reyes-Uribe et al., 2018). However, due to the limitations of our CRISPR-Cas9 experimental design and focus on later time points, further studies to investigate the mechanism of immediate cellular effects following reduction - or elimination - of GABPβ1L function in *TERT* promoter mutant GBM will require inducible systems and single-cell analysis.

GABPβ1L tetramerization activity and *TERT* expression were reduced but not eliminated in our experiments. Attempts to further suppress *TERT* mRNA expression in the GABPβ1L-reduced clones through LNA-ASO-mediated knockdown of GABPβ1L had no effect. Therefore, a low level of expression of *TERT* from the mutant promoter may be maintained independent of GABPβ1L function. Although our data strongly support GABPβ1L as the main driver of *TERT* expression from the mutant promoter and the primary factor enabling cell immortality in *TERT* promoter mutant GBM, they also support the existence of a secondary mechanism contributing to the overall *TERT* expression level in *TERT* promoter mutant tumor cells. Secondary mechanisms could involve an activating structural change in the mutant *TERT* promoter G-quadruplex or activation through recruitment of other ETS factors (Chaires et al., 2014; Li et al., 2015; Lim et al., 2010; Makowski et al., 2016).

Additionally, the GABP tetramer-forming isoform GABPβ2 may be able to partially activate *TERT* expression at the mutant *TERT* promoter. GABPβ2 knockdown significantly reduced *TERT* expression levels in a subset of *TERT* promoter mutant GBM lines. However, the absence of a positive correlation between *GABPB2* and *TERT* expression levels in glioma tissue samples and the near total loss of the occupancy of GABP at the mutant *TERT* promoter after disruption of GABPβ1L suggest that GABPβ2 plays a more minor role, at least when GAPβ1L is present. We cannot however exclude the possibility that GABPβ2 plays a role in regulating the mutant *TERT* promoter in a small subset of cells. Therefore, to fully eliminate *TERT* expression in *TERT* promoter GBM, it may be necessary to jointly inhibit GABPβ1L alongside one or more secondary mechanisms of *TERT* expression.

5.3 GABPβ1L AS A THERAPEUTIC TARGET IN CANCER

Overall, the present study gives credence to GABPβ1L as a potential therapeutic target for tumor cells with the mutant *TERT* promoter. GABP is recruited to the mutant *TERT* promoter in multiple cancer types (Akincilar et al., 2016; Bell et al., 2015; Stern et al., 2015) and therefore may be universal therapeutic target for *TERT* promoter mutant tumors.

The prevalence of identical *TERT* promoter mutations across a large number of cancer types (Bell et al., 2016; Zehir et al., 2017) highlights the potentially widespread role of the GABPβ1L-containing GABP tetramer as a dominant factor responsible for enabling replicative immortality in cancer. This is particularly relevant as direct telomerase inhibitors block tumor cell immortality, but can also affect *TERT* in normal stem and germ cells (Jager and Walter, 2016; Shay and Wright, 2006). Although GABP is a transcription factor, it is an intriguing target due to its dual function as a dimer and tetramer. GABPβ1L is not required for normal development in mice, and in GBM cells the majority of GABP target genes do not seem to be as sensitive to reduction of GABPβ1L compared to the mutant *TERT* promoter. Thus, inhibiting the dispensable tetramer-forming GABPβ1L isoform while leaving the dimer and other cell-essential GABP isoforms unperturbed could be a viable strategy to block cellular immortality in *TERT* promoter mutant tumors, including glioma.

REFERENCES

Akincilar, S., Khattar, E., Boon, P. L., Unal, B., Fullwood, M. J., and Tergaonkar, V. (2016). Long-range chromatin interactions drive mutant Tert promoter activation. Cancer Discov.

Arita, H., Narita, Y., Fukushima, S., Tateishi, K., Matsushita, Y., Yoshida, A., Miyakita, Y., Ohno, M., Collins, V. P., Kawahara, N.*, et al.* (2013). Upregulating mutations in the TERT promoter commonly occur in adult malignant gliomas and are strongly associated with total 1p19q loss. Acta neuropathologica *126*, 267-276.

Barszczyk, M., Buczkowicz, P., Castelo-Branco, P., Mack, S. C., Ramaswamy, V., Mangerel, J., Agnihotri, S., Remke, M., Golbourn, B., Pajovic, S.*, et al.* (2014). Telomerase inhibition abolishes the tumorigenicity of pediatric ependymoma tumor-initiating cells. Acta neuropathologica *128*, 863-877.

Bell, R. J., Rube, H. T., Kreig, A., Mancini, A., Fouse, S. D., Nagarajan, R. P., Choi, S., Hong, C., He, D., Pekmezci, M.*, et al.* (2015). Cancer. The transcription factor GABP selectively binds and activates the mutant TERT promoter in cancer. Science *348*, 1036-1039.

Bell, R. J., Rube, H. T., Xavier-Magalhaes, A., Costa, B. M., Mancini, A., Song, J. S., and Costello, J. F. (2016). Understanding TERT Promoter Mutations: A Common Path to Immortality. Molecular cancer research : MCR *14*, 315-323.

Blackburn, E. H., Greider, C. W., and Szostak, J. W. (2006). Telomeres and telomerase: the path from maize, Tetrahymena and yeast to human cancer and aging. Nat Med *12*, 1133-1138.

Brown, A., Woods, W. S., and Perez-Pinera, P. (2016). Multiplexed Targeted Genome Engineering Using a Universal Nuclease-Assisted Vector Integration System. ACS Synth Biol *5*, 582-588.

Bryan, T. M., and Cech, T. R. (1999). Telomerase and the maintenance of chromosome ends. Current opinion in cell biology *11*, 318-324.

Cancer Genome Atlas Research, N. (2008). Comprehensive genomic characterization defines human glioblastoma genes and core pathways. Nature *455*, 1061-1068.

Cao, Y., Li, H., Deb, S., and Liu, J. P. (2002). TERT regulates cell survival independent of telomerase enzymatic activity. Oncogene *21*, 3130-3138.

Capper, R., Britt-Compton, B., Tankimanova, M., Rowson, J., Letsolo, B., Man, S., Haughton, M., and Baird, D. M. (2007). The nature of telomere fusion and a definition of the critical telomere length in human cells. Genes & development *21*, 2495-2508.

Carter, R. S., and Avadhani, N. G. (1994). Cooperative binding of GA-binding protein transcription factors to duplicated transcription initiation region repeats of the cytochrome c oxidase subunit IV gene. J Biol Chem *269*, 4381-4387.

Castelo-Branco, P., Zhang, C., Lipman, T., Fujitani, M., Hansford, L., Clarke, I., Harley, C. B., Tressler, R., Malkin, D., Walker, E.*, et al.* (2011). Neural tumor-initiating cells have distinct telomere maintenance and can be safely targeted for telomerase inhibition. Clinical cancer research : an official journal of the American Association for Cancer Research *17*, 111-121.

Cawthon, R. M. (2002). Telomere measurement by quantitative PCR. Nucleic acids research *30*, e47.

Ceccarelli, M., Barthel, F. P., Malta, T. M., Sabedot, T. S., Salama, S. R., Murray, B. A., Morozova, O., Newton, Y., Radenbaugh, A., Pagnotta, S. M., *et al.* (2016). Molecular Profiling Reveals Biologically Discrete Subsets and Pathways of Progression in Diffuse Glioma. Cell *164*, 550-563.

Chaires, J. B., Trent, J. O., Gray, R. D., Dean, W. L., Buscaglia, R., Thomas, S. D., and Miller, D. M. (2014). An improved model for the hTERT promoter quadruplex. PLoS One *9*, e115580.

Chiba, K., Johnson, J. Z., Vogan, J. M., Wagner, T., Boyle, J. M., and Hockemeyer, D. (2015). Cancer-associated TERT promoter mutations abrogate telomerase silencing. Elife *4*.

Chiba, K., Lorbeer, F. K., Shain, A. H., McSwiggen, D. T., Schruf, E., Oh, A., Ryu, J., Darzacq, X., Bastian, B. C., and Hockemeyer, D. (2017). Mutations in the promoter of the telomerase gene TERT contribute to tumorigenesis by a two-step mechanism. Science *357*, 1416-1420.

Chin, L., Artandi, S. E., Shen, Q., Tam, A., Lee, S. L., Gottlieb, G. J., Greider, C. W., and DePinho, R. A. (1999). p53 deficiency rescues the adverse effects of telomere loss and cooperates with telomere dysfunction to accelerate carcinogenesis. Cell *97*, 527-538.

Chinenov, Y., Henzl, M., and Martin, M. E. (2000). The alpha and beta subunits of the GA-binding protein form a stable heterodimer in solution. Revised model of heterotetrameric complex assembly. The Journal of biological chemistry *275*, 7749-7756.

Counter, C. M., Avilion, A. A., LeFeuvre, C. E., Stewart, N. G., Greider, C. W., Harley, C. B., and Bacchetti, S. (1992). Telomere shortening associated with chromosome instability is arrested in immortal cells which express telomerase activity. The EMBO journal *11*, 1921-1929.

Counter, C. M., Meyerson, M., Eaton, E. N., Ellisen, L. W., Caddle, S. D., Haber, D. A., and Weinberg, R. A. (1998). Telomerase activity is restored in human cells by ectopic expression of hTERT (hEST2), the catalytic subunit of telomerase. Oncogene *16*, 1217-1222.

de la Brousse, F. C., Birkenmeier, E. H., King, D. S., Rowe, L. B., and McKnight, S. L. (1994). Molecular and genetic characterization of GABP beta. Genes & development *8*, 1853-1865.

Deeraksa, A., Pan, J., Sha, Y., Liu, X. D., Eissa, N. T., Lin, S. H., and Yu-Lee, L. Y. (2013). Plk1 is upregulated in androgen-insensitive prostate cancer cells and its inhibition leads to necroptosis. Oncogene *32*, 2973-2983.

der-Sarkissian, H., Bacchetti, S., Cazes, L., and Londono-Vallejo, J. A. (2004). The shortest telomeres drive karyotype evolution in transformed cells. Oncogene *23*, 1221-1228.

Donadini, A., Giacopelli, F., Ravazzolo, R., Gandin, V., Marchisio, P. C., and Biffo, S. (2006). GABP complex regulates transcription of eIF6 (p27BBP), an essential trans-acting factor in ribosome biogenesis. FEBS Lett *580*, 1983-1987.

Fitzgerald, M. S., Riha, K., Gao, F., Ren, S., McKnight, T. D., and Shippen, D. E. (1999). Disruption of the telomerase catalytic subunit gene from Arabidopsis inactivates telomerase and leads to a slow loss of telomeric DNA. Proceedings of

the National Academy of Sciences of the United States of America *96*, 14813-14818.

Fouse, S. D., Nakamura, J. L., James, C. D., Chang, S., and Costello, J. F. (2014). Response of primary glioblastoma cells to therapy is patient specific and independent of cancer stem cell phenotype. Neuro-oncology *16*, 361-371.

Fragkos, M., and Beard, P. (2011). Mitotic catastrophe occurs in the absence of apoptosis in p53-null cells with a defective G1 checkpoint. PLoS One *6*, e22946.

Gapinske, M., Tague, N., Winter, J., Underhill, G. H., and Perez-Pinera, P. (2018). Targeted Gene Knock Out Using Nuclease-Assisted Vector Integration: Hemi- and Homozygous Deletion of JAG1. Methods Mol Biol *1772*, 233-248.

Genuario, R. R., and Perry, R. P. (1996). The GA-binding protein can serve as both an activator and repressor of ribosomal protein gene transcription. J Biol Chem *271*, 4388-4395.

Hackett, J. A., Feldser, D. M., and Greider, C. W. (2001). Telomere dysfunction increases mutation rate and genomic instability. Cell *106*, 275-286.

Hayashi, M. T., Cesare, A. J., Rivera, T., and Karlseder, J. (2015). Cell death during crisis is mediated by mitotic telomere deprotection. Nature *522*, 492-496.

Horn, S., Figl, A., Rachakonda, P. S., Fischer, C., Sucker, A., Gast, A., Kadel, S., Moll, I., Nagore, E., Hemminki, K.*, et al.* (2013). TERT promoter mutations in familial and sporadic melanoma. Science *339*, 959-961.

Hsu, P. D., Scott, D. A., Weinstein, J. A., Ran, F. A., Konermann, S., Agarwala, V., Li, Y., Fine, E. J., Wu, X., Shalem, O.*, et al.* (2013). DNA targeting specificity of RNA-guided Cas9 nucleases. Nat Biotechnol *31*, 827-832.

Huang, F. W., Hodis, E., Xu, M. J., Kryukov, G. V., Chin, L., and Garraway, L. A. (2013). Highly recurrent TERT promoter mutations in human melanoma. Science *339*, 957-959.

Ianzini, F., and Mackey, M. A. (1997). Spontaneous premature chromosome condensation and mitotic catastrophe following irradiation of HeLa S3 cells. Int J Radiat Biol *72*, 409-421.

Iwado, E., Daido, S., Kondo, Y., and Kondo, S. (2007). Combined effect of 2-5A-linked antisense against telomerase RNA and conventional therapies on human malignant glioma cells in vitro and in vivo. International journal of oncology *31*, 1087-1095.

Jager, K., and Walter, M. (2016). Therapeutic Targeting of Telomerase. Genes *7*.

Jing, X., Zhao, D. M., Waldschmidt, T. J., and Xue, H. H. (2008). GABPbeta2 is dispensible for normal lymphocyte development but moderately affects B cell responses. J Biol Chem *283*, 24326-24333.

Killela, P. J., Reitman, Z. J., Jiao, Y., Bettegowda, C., Agrawal, N., Diaz, L. A., Jr., Friedman, A. H., Friedman, H., Gallia, G. L., Giovanella, B. C.*, et al.* (2013). TERT promoter mutations occur frequently in gliomas and a subset of tumors derived from cells with low rates of self-renewal. Proceedings of the National Academy of Sciences of the United States of America *110*, 6021-6026.

Kim, N. W., Piatyszek, M. A., Prowse, K. R., Harley, C. B., West, M. D., Ho, P. L., Coviello, G. M., Wright, W. E., Weinrich, S. L., and Shay, J. W. (1994). Specific association of human telomerase activity with immortal cells and cancer. Science *266*, 2011-2015.

Li, Y., Zhou, Q. L., Sun, W., Chandrasekharan, P., Cheng, H. S., Ying, Z., Lakshmanan, M., Raju, A., Tenen, D. G., Cheng, S. Y.*, et al.* (2015). Non-canonical NF-kappaB signalling and ETS1/2 cooperatively drive C250T mutant TERT promoter activation. Nat Cell Biol *17*, 1327-1338.

Lim, K. W., Lacroix, L., Yue, D. J., Lim, J. K., Lim, J. M., and Phan, A. T. (2010). Coexistence of two distinct G-quadruplex conformations in the hTERT promoter. J Am Chem Soc *132*, 12331-12342.

Lin, J., Epel, E., Cheon, J., Kroenke, C., Sinclair, E., Bigos, M., Wolkowitz, O., Mellon, S., and Blackburn, E. (2010). Analyses and comparisons of telomerase activity and telomere length in human T and B cells: insights for epidemiology of telomere maintenance. J Immunol Methods *352*, 71-80.

Makowski, M. M., Willems, E., Fang, J., Choi, J., Zhang, T., Jansen, P. W., Brown, K. M., and Vermeulen, M. (2016). An interaction proteomics survey of transcription factor binding at recurrent TERT promoter mutations. Proteomics *16*, 417-426.

Marian, C. O., Cho, S. K., McEllin, B. M., Maher, E. A., Hatanpaa, K. J., Madden, C. J., Mickey, B. E., Wright, W. E., Shay, J. W., and Bachoo, R. M. (2010). The telomerase antagonist, imetelstat, efficiently targets glioblastoma tumor-initiating cells leading to decreased proliferation and tumor growth. Clinical cancer research : an official journal of the American Association for Cancer Research *16*, 154-163.

Meyerson, M., Counter, C. M., Eaton, E. N., Ellisen, L. W., Steiner, P., Caddle, S. D., Ziaugra, L., Beijersbergen, R. L., Davidoff, M. J., Liu, Q.*, et al.* (1997). hEST2,

the putative human telomerase catalytic subunit gene, is up-regulated in tumor cells and during immortalization. Cell *90*, 785-795.

Ohba, S., Mukherjee, J., Johannessen, T. C., Mancini, A., Chow, T. T., Wood, M., Jones, L., Mazor, T., Marshall, R. E., Viswanath, P.*, et al.* (2016). Mutant IDH1 Expression Drives TERT Promoter Reactivation as Part of the Cellular Transformation Process. Cancer Res *76*, 6680-6689.

Reyes-Uribe, P., Adrianzen-Ruesta, M. P., Deng, Z., Echevarria-Vargas, I., Mender, I., Saheb, S., Liu, Q., Altieri, D. C., Murphy, M. E., Shay, J. W.*, et al.* (2018). Exploiting TERT dependency as a therapeutic strategy for NRAS-mutant melanoma. Oncogene.

Rosmarin, A. G., Resendes, K. K., Yang, Z., McMillan, J. N., and Fleming, S. L. (2004). GA-binding protein transcription factor: a review of GABP as an integrator of intracellular signaling and protein-protein interactions. Blood Cells Mol Dis *32*, 143-154.

Saretzki, G., Sitte, N., Merkel, U., Wurm, R. E., and von Zglinicki, T. (1999). Telomere shortening triggers a p53-dependent cell cycle arrest via accumulation of G-rich single stranded DNA fragments. Oncogene *18*, 5148-5158.

Sawada, J., Goto, M., Sawa, C., Watanabe, H., and Handa, H. (1994). Transcriptional activation through the tetrameric complex formation of E4TF1 subunits. EMBO J *13*, 1396-1402.

Shay, J. W., and Wright, W. E. (2000). Hayflick, his limit, and cellular ageing. Nat Rev Mol Cell Biol *1*, 72-76.

Shay, J. W., and Wright, W. E. (2006). Telomerase therapeutics for cancer: challenges and new directions. Nat Rev Drug Discov *5*, 577-584.

Spiegl-Kreinecker, S., Lotsch, D., Ghanim, B., Pirker, C., Mohr, T., Laaber, M., Weis, S., Olschowski, A., Webersinke, G., Pichler, J., and Berger, W. (2015). Prognostic quality of activating TERT promoter mutations in glioblastoma: interaction with the rs2853669 polymorphism and patient age at diagnosis. Neuro-oncology *17*, 1231-1240.

Stern, J. L., Theodorescu, D., Vogelstein, B., Papadopoulos, N., and Cech, T. R. (2015). Mutation of the TERT promoter, switch to active chromatin, and monoallelic TERT expression in multiple cancers. Genes & development *29*, 2219-2224.

Vakifahmetoglu, H., Olsson, M., and Zhivotovsky, B. (2008). Death through a tragedy: mitotic catastrophe. Cell Death Differ *15*, 1153-1162.

Vinagre, J., Almeida, A., Populo, H., Batista, R., Lyra, J., Pinto, V., Coelho, R., Celestino, R., Prazeres, H., Lima, L.*, et al.* (2013). Frequency of TERT promoter mutations in human cancers. Nat Commun *4*, 2185.

Vitale, I., Galluzzi, L., Castedo, M., and Kroemer, G. (2011). Mitotic catastrophe: a mechanism for avoiding genomic instability. Nat Rev Mol Cell Biol *12*, 385-392.

Wang, F., Pan, X., Kalmbach, K., Seth-Smith, M. L., Ye, X., Antumes, D. M., Yin, Y., Liu, L., Keefe, D. L., and Weissman, S. M. (2013). Robust measurement of telomere length in single cells. Proceedings of the National Academy of Sciences of the United States of America *110*, E1906-1912.

Whitaker, N. J., Bryan, T. M., Bonnefin, P., Chang, A. C., Musgrove, E. A., Braithwaite, A. W., and Reddel, R. R. (1995). Involvement of RB-1, p53, p16INK4 and telomerase in immortalisation of human cells. Oncogene *11*, 971-976.

Xie, Z., Jay, K. A., Smith, D. L., Zhang, Y., Liu, Z., Zheng, J., Tian, R., Li, H., and Blackburn, E. H. (2015). Early telomerase inactivation accelerates aging independently of telomere length. Cell *160*, 928-939.

Xu, M., Lee, E. M., Wen, Z., Cheng, Y., Huang, W. K., Qian, X., Tcw, J., Kouznetsova, J., Ogden, S. C., Hammack, C.*, et al.* (2016). Identification of small-molecule inhibitors of Zika virus infection and induced neural cell death via a drug repurposing screen. Nat Med *22*, 1101-1107.

Xue, H. H., Jing, X., Bollenbacher-Reilley, J., Zhao, D. M., Haring, J. S., Yang, B., Liu, C., Bishop, G. A., Harty, J. T., and Leonard, W. J. (2008). Targeting the GA binding protein beta1L isoform does not perturb lymphocyte development and function. Mol Cell Biol *28*, 4300-4309.

Yang, Z. F., Drumea, K., Mott, S., Wang, J., and Rosmarin, A. G. (2014). GABP transcription factor (nuclear respiratory factor 2) is required for mitochondrial biogenesis. Mol Cell Biol *34*, 3194-3201.

Yang, Z. F., Mott, S., and Rosmarin, A. G. (2007). The Ets transcription factor GABP is required for cell-cycle progression. Nature cell biology *9*, 339-346.

Yu, M., Yang, X. Y., Schmidt, T., Chinenov, Y., Wang, R., and Martin, M. E. (1997). GA-binding protein-dependent transcription initiator elements. Effect of helical spacing between polyomavirus enhancer a factor 3(PEA3)/Ets-binding sites on initiator activity. J Biol Chem *272*, 29060-29067.

Yu, S., Jing, X., Colgan, J. D., Zhao, D. M., and Xue, H. H. (2012). Targeting tetramer-forming GABPbeta isoforms impairs self-renewal of hematopoietic and leukemic stem cells. Cell Stem Cell *11*, 207-219.

Zehir, A., Benayed, R., Shah, R. H., Syed, A., Middha, S., Kim, H. R., Srinivasan, P., Gao, J., Chakravarty, D., Devlin, S. M.*, et al.* (2017). Mutational landscape of metastatic cancer revealed from prospective clinical sequencing of 10,000 patients. Nat Med *23*, 703-713.

Publishing Agreement

It is the policy of the University to encourage the distribution of all theses, dissertations, and manuscripts. Copies of all UCSF theses, dissertations, and manuscripts will be routed to the library via the Graduate Division. The library will make all theses, dissertations, and manuscripts accessible to the public and will preserve these to the best of their abilities, in perpetuity.

I hereby grant permission to the Graduate Division of the University of California, San Francisco to release copies of my thesis, dissertation, or manuscript to the Campus Library to provide access and preservation, in whole or in part, in perpetuity.

Author Signature Andrew G. Marcini Date 10/15/18